ADAPTIVE CHANNEL ESTIMATION AND FREQUENCY DOMAIN CHANNEL EQUALIZATION IN DS-CDMA/OFDM COMPOSITE RADIO ENVIRONMENT FOR SOFTWARE DEFINED RADIO RECEIVERS

TIANQI WANG

Adaptive Channel Estimation and Frequency Domain Channel Equalization in DS-CDMA/OFDM Composite Radio Environment for Software Defined Radio Receivers

by

© Tianqi Wang
Master of Engineering

A thesis submitted to the
School of Graduate Studies
in partial fulfillment of the
requirements for the degree of
Master of Engineering.

Department of Electrical and Computer Engineering
Memorial University of Newfoundland

May 8, 2007

ST. JOHN'S NEWFOUNDLAND

Contents

Abstract

The main contribution of this thesis is the successful development of a generic frequency domain equalizer (FDE)-based receiver architecture aiming at the application in the DS-CDMA/OFDM composite radio environment. The proposed receiver architecture featuring low-cost and good performance has great potential to be implemented via software defined radio (SDR) technology.

Firstly, we present a brief introduction to the SDR technology, including software architecture and hardware architecture. Secondly, the system models for direct sequence code division multiple access (DS-CDMA) systems and Orthogonal Frequency Division Multiplexing (OFDM) systems are introduced. Moreover,as the theoretical basis, some important wireless channel models are provided and analyzed.

Utilizing the existing channel models, a frequency domain adaptive estimation of Doppler shifts for multiple Doppler subpaths in DS-CDMA systems is proposed. By modeling the doubly selective channel using a basis expansion model (BEM), the proposed Expectation-Maximization (EM) algorithm-based estimation method can obtain accurate information of Doppler shifts. Moreover, we propose an iterative algorithm for frequency domain joint estimation of synchronization parameter and channel impulse response (CIR) in DS-CDMA systems. Based on the estimated information of Doppler shifts, synchronization parameter, and CIR, an FDE-based receiver architecture is developed to exploit Doppler diversity in the frequency do-

main. The proposed estimation algorithm can be easily migrated for the application in OFDM systems with minor modifications. Based on the proposed frequency domain channel estimation scheme, a generic frequency domain equalizer (FDE)-based receiver architecture is eventually proposed. This architecture can be readily implemented by the SDR technology. Our results manifest that this receiver architecture is promising and can achieve good performance with low cost.

Acknowledgements

I would like to thank all of you who have given your time, assistance and patience so generously. I am very grateful to my supervisor, Cheng Li, for his feedback and for keeping me focussed in my research. The consistent trust and support from Dr. Cheng Li greatly encouraged me to improve my work. My appreciation also goes to my co-supervisor, Mohamed Hossam Ahmed, whose invaluable expertise greatly helps me turn my idea into reality.

It has been a pleasure to study at the Computer Engineering Research Laboratory (CERL) in Memorial University of Newfoundland during these years. Special thanks to Ling Wu, Pu Wang, Liang Zhang, and Guan Wang for the precious friendship and generous support.

I am also indebted to my parents. Thank you for your unending support, willingness to accept and eagerness to love.

Thanks to Shenqiu Zhang for the selfless support she has been giving to me. Thank you for saving me from all the depressions and anxieties I have went through.

Last but not least I would like to acknowledge Reza Shahidi for his large responsibility for the outstanding computer facilities we have in CERL.

List of Symbols

The following assumptions and definitions are used in this thesis.

- Vectors and matrices are denoted in bold fonts with overline, such as $\overline{\mathbf{A}}, \overline{\mathbf{B}}$.
- The symbol $*$ is used to denote matrix multiplication.
- The symbol $\otimes$ is used to denote convolution.
- $\{\cdot\}^T$ stands for transpose matrix.
- $\{\cdot\}^H$ and $\{\cdot\}^{(-1)}$ denote conjugate transpose matrix and inverse matrix, respectively.
- $\mathbf{E}\{\cdot\}$ denotes the expectation of random variables.
- $diag\{a_0, a_1, \cdots, a_K\}$ denotes a diagonal matrix with elements $\{a_0, a_1, \cdots, a_K\}$ on the main diagonal.
- $\{\cdot\}^*$ denotes conjugate operation.
- $|\cdot|$ denotes the operation of returning the absolute value.
- $\lceil\cdot\rceil$ denotes the operation of returning the ceiling of a number.

- $\Re\{\cdot\}$ and $\Im\{\cdot\}$ denote the operation of returning the real value and imaginary value of a complex number, respectively.
- j denotes $\sqrt{-1}$.
- N_r denotes time-dependent additive white Gaussian noise (AWGN), whose expectation $\mathbf{E}\{N_r\} = 0$.
- σ_N^2 denotes the standard deviation of N_r, which means $\mathbf{E}\{|N_r|^2\} = \sigma_N^2$

List of Tables

List of Figures

Chapter 1

Introduction

1.1 Basic Concepts of Software Defined Radio Technology

As an emerging technology which is aimed at adaptively utilizing the radio spectrum resource, cognitive radio (CR) has attracted broad studies in recent years [6]. The main feature of a typical cognitive radio receiver is that it can automatically identify and allocate available radio frequency spectrum resources without infringing the rights and interfering with the operations of licensed users. From the definition of cognitive radio, it is obvious that the very fundamental issue of an ideal CR receiver lies in a reconfigurable receiver architecture, which is able to adapt to various communications environments with minimum latency. Therefore, a flexible and powerful implementation technology of radio receiver is desired for the realization of cognitive radio. The software defined radio (SDR) technology has now been widely accepted as the choice for implementation.

A software defined radio is a radio that is substantially defined in software and

whose physical behavior, such as data rate, carrier frequency, coding scheme, etc. can be significantly altered through the changes in its software [7]. For example, a radio, which defines its modulation/demodulation, synchronization, and coding/decoding in its software and can switch between different protocols, can be viewed as a software defined radio. On the other hand, a radio built on microprocessor/DSPs is not necessarily a software defined radio, if the programmable hardware platform is used only for providing entertainment software rather than physical behavior. The essence of the software defined radio is that the physical behavior can be fully defined and controlled by software.

The SDR forum defines five tiers of solutions which describe the development of software defined radio in details [8]. Tier 0 is a traditional radio implementation in hardware. Tier 1 is software-controlled radio (SCR), which implements the control features for multiple hardware elements in software. Tier 2 implements modulation and baseband processing in software but allows for multiple frequency-fixed functions realized in RF hardware. This tier is SDR. Tier3, ideal software radio (ISR), provides programmability in radio frequency (RF) stage and places separate analog conversion in the antenna. Tier 4, ultimate software radio (USR), can realize fast transitions between communication protocols with advanced digital processing capability.

SDR has attracted a lot of research interests for the following reasons:

1. **Time-to-market can be greatly shortened.** The traditional hardware implementation of radio receiver needs a long development cycle. However, as the wireless communication technologies are changing rapidly, this approach becomes no longer suitable. The SDR platform provides programmable hardware architecture and generic application programming interfaces (APIs). Therefore, the SDR receiver can be upgraded to support new algorithms and new schemes

simply by updating the software. The development cycle can be significantly reduced.

2. **Various standards can be seamlessly supported.** The co-existence of various wireless communications standards, such as General Packet Radio Service (GPRS), Universal Mobile Telecommunications System (UMTS), and Wireless Local Area Network (WLAN), has made SDR attractive. Traditionally, they are incompatible and independent from each other, therefore, dedicated hardware for different standards would be required. With powerful control functions and compatibility of software, the SDR technology greatly facilitates the internetworking between different networks. This further enables the seamless support of various standards via SDR.

3. **Various levels of services can be provided flexibly.** The telecommunication carriers may provide different services and QoS levels according to the requirements of users. Through the SDR technology, service parameters can be easily modified (such as data rate, coding/decoding schedule, etc) to adjust the QoS level correspondingly. Moreover, uses can enjoy the latest service by simply downloading software from the service providers.

4. **Significant cost saving.** Compared to the costly new dedicated hardware development, software development approach is more cost-efficient for the manufacturers. From the users' perspective, they do not need to purchase different devices to access different communication networks. The SDR technology provides the flexibility in universal access and future-proof solutions.

An ideal SDR is expected to possess the following characteristics: multi-functionality, global mobility, compactness, power efficiency, and ease of manufacture [7]. A generic

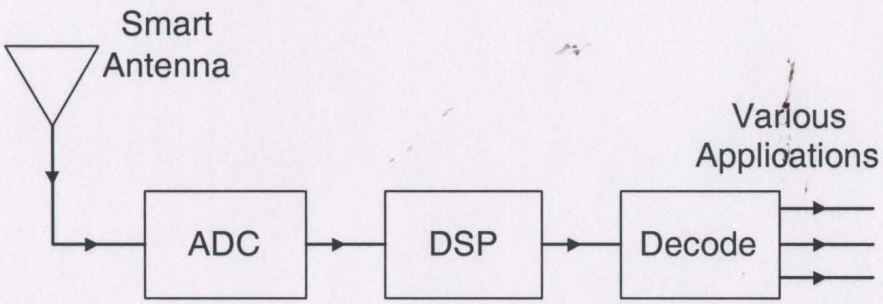

Figure 1.1: A generic SDR receiver structure

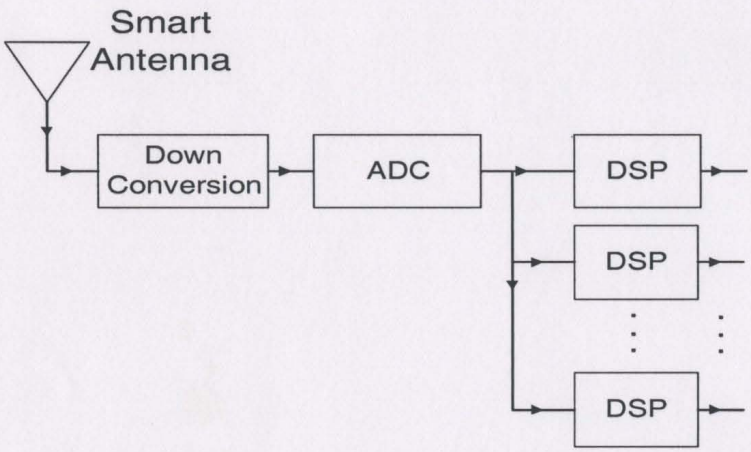

Figure 1.2: A generic SDR receiver structure for practical applications

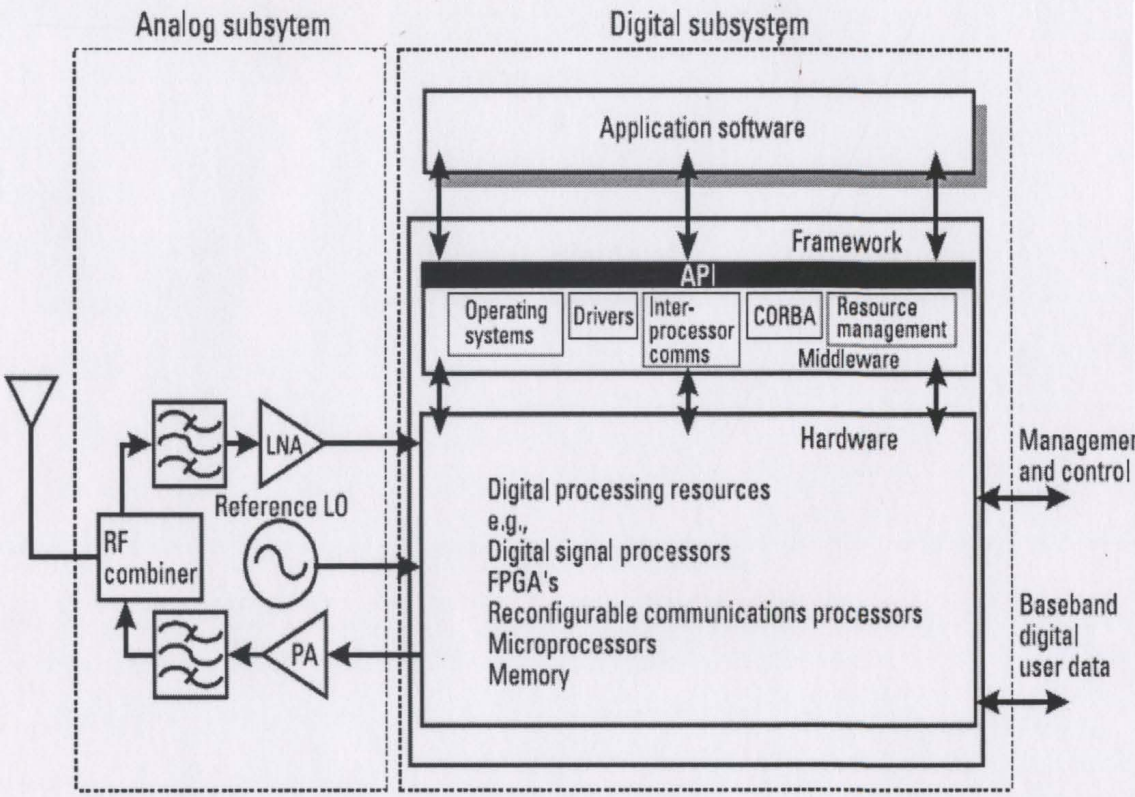

Figure 1.3: The illustration of the architecture used in a typical SDR receiver (taken from Page 4 of [1])

block diagram of the hardware platform of an ideal SDR receiver is shown in Fig. 1.1. As shown in the figure, the received analog signal from the antenna will be sampled by the *Analog to Digital Converter* (ADC) directly during the radio frequency (RF) stage. The rest of the signal processing tasks will be carried out in the digital domain using software running on high-speed DSP processors. Therefore, extremely high-speed ADC devices would be required, which usually becomes the bottleneck of the system design. Therefore, as shown in Fig. 1.2, instead of directly sampling the received signal at the RF stage, a *Down-Conversion* module is often adopted before the ADC for practical reasons. In this way, the sampling procedure can be conducted at the intermediate frequency (IF) stage. As shown in Fig. 1.2, for a practical SDR receiver, multiple DSP processors are often used to execute digital signal processing algorithms in parallel.

A more detailed illustration of the architecture is shown in Fig. 1.3. It can be observed that the hardware system of a typical SDR receiver consists of two subsystems: analog subsystem and digital subsystem. The analog subsystem has components which can not be realized in digital circuits, such as an antenna, RF filter, power amplification, and etc. However, as the digitalization of the SDR system is moving closer to the antenna, the analog subsystem will become simpler in the future. At the same time, even with current technology, all baseband signal processing (channel encoding/decoding, modulation/demodulation, and channel estimation) can readily be implemented in the digital subsystem.

As shown in Fig. 1.3, the digital subsystem can be further divided into three layers: the software layer, the middleware layer, and the hardware layer. By using the middleware layer, hardware resources can be completely separated from the application software. The middleware layer abstracts hardware elements as objects and provides communications between different hardware objects via standard interfaces.

Therefore, the middleware layer forms the basis on which all the application software is built. That is why the middleware layer can also be referred to as the "Software Architecture." In Section 1.2, a brief review of the most broadly accepted software architecture for SDR receivers will be given. In Section 1.3, we will briefly compare several popular hardware platforms for SDR receivers. Finally, based on a generic estimation and equalization algorithm, we will present a SDR receiver architecture operating in the DS-CDMA/OFDM composite radio environment. This architecture and the proposed generic frequency domain channel estimation and equalization scheme will be fully studied in the following chapters.

1.2 Software Architecture of Software Defined Radio Receivers

Object-oriented programming languages, such as C++ and Java, have been widely used to facilitate the development of the software defined radio. The adoption of the concept of object allows the easy reuse of hardware resources. Moreover, by using abstract classes, a framework facilitating the system integration can be easily created. However, the framework constructed by simple abstract classes has some limitations. For example, it assumes that all objects interfacing with each other should exist in the same address space [7]. This limits the applications of framework in distributed systems. Therefore, a more powerful, platform-independent framework is highly desired.

Common Object Request Broker Architecture (CORBA) is the most successful framework used in SDR receivers by far. CORBA is proposed by the Object Management Group (OMG). The goal is to provide the objects in distributed systems

which can interact with each other seamlessly across communications media that are transparent to the developer. The development of two objects are usually involved, namely, the client and server objects, where the client object is defined as the object that requests a service and the server object is the object that performs the service requested by the client object. The core of CORBA is the Object Request Broker (ORB). More details of CORBA and ORB related issues can be found in the official home page of OMG [9].

Based on the CORBA framework, the U.S. Department of Defense proposed a Joint Tactical Radio System (JTRS), in which a software communication architecture (SCA) is used. The initial target of JTRS is to integrate a large and sophisticated set of communications systems. Now, JTRS has been further developed to increase the flexibility and interoperability of various communications systems around the world. Due to the outstanding performance of JTRS, more and more commercial SDR receivers have been designed as JTRS-compliant devices.

The SCA plays an important role in the success of JTRS. The main features of SCA include allowing the portability of different SCA implementations, providing an object-oriented framework, adopting Commercial-Off-The-Shelf (COTS) components, etc. [7]. The SCA defines the operating environment (OE) for radio systems, including necessary services and interfaces. The overall structure of SCA is shown in Fig. 1.4 [2]. From the figure, we can see that the core framework (CF) of SCA is a logical software bus via CORBA by using the Interface Description Language (IDL). Various components of a SDR transceiver are built on the CF. The communication among them are supported by the CF through well-defined APIs.

As given in [2], all applications are comprised of *Resources* and *Devices*. In an ideal SDR receiver, all the needed entities can be classified into six categories: *ModemDevice*, *LinkResource*, *SecurityDevice*, *NetworkResource*, *I/ODevice*, and *Util-*

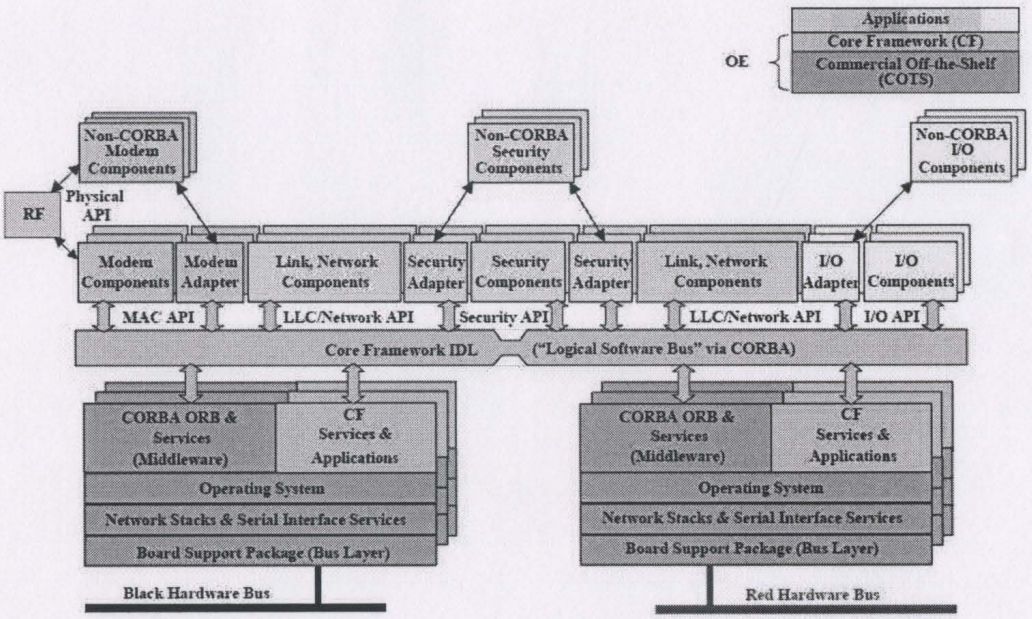

Figure 1.4: The illustration of the SCA structure (taken from Page 2-2 of [2])

ityResource. Detailed information of the classifications and subcategories can be found in [2]. We take the *ModemDevice* as an example to briefly illustrate the relationships among various entities. As shown in Fig. 1.5, the *ModemDevice* provides Physical/MAC layer applications and needs the resources released by the *LinkResource* entity. The *ModemDevice* is in fact defined as a parent class of multiple child classes: *ModemAdapterDevice*, *WaveformModemDevice*, *WaveformRFAdapterDevice*, and *RepeaterAdapterDevice*. The functionalities of the *ModemDevice* can be further divided and assigned to these child classes. All the entities defined in SDR

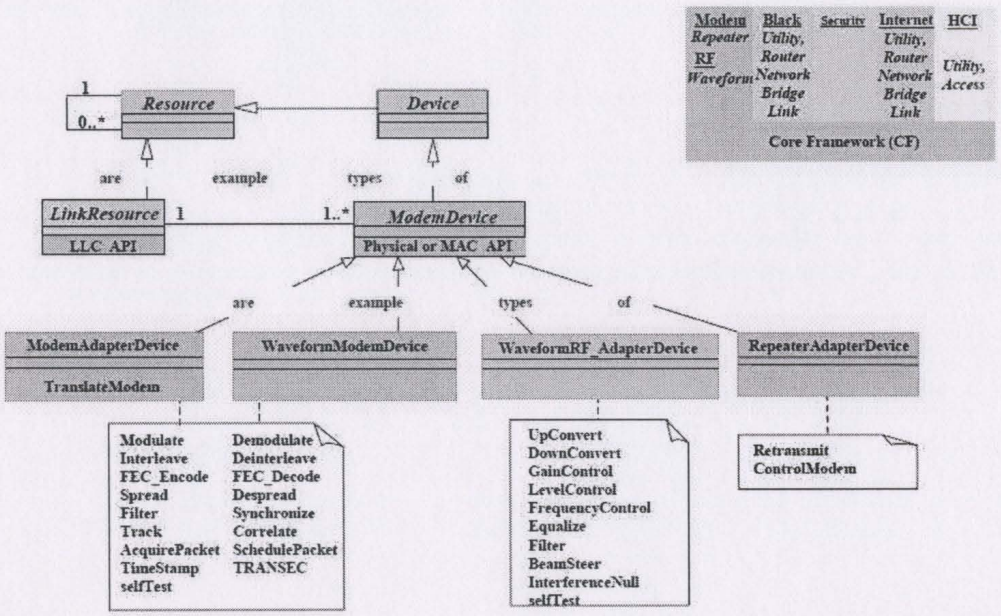

Figure 1.5: The illustration of the *ModemResources* entity (taken from Page 2-8 of [2])

receivers have attributes and behaviors, although for some entities, the attributes and/or behaviors are not necessarily defined [2]. For example, as shown in Fig. 1.5,

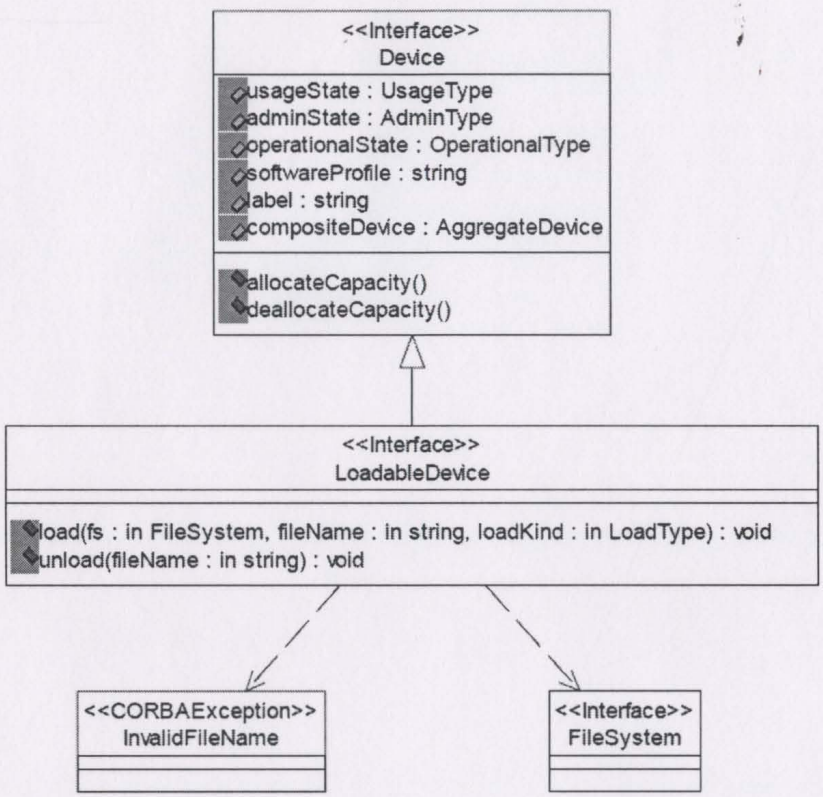

Figure 1.6: The UML description of the interfaces of the *LoadableDevice*(taken from Page 3-63 of [2])

the *WaveformRFAdapterDevice* entity has the behavior *Equalize* to provide equalization functionality for the receiver. In the SCA regulation, the interfaces of entities are depicted using the Unified Modeling Language (UML). An example of the UML definition of a *LoadableDevice* is shown in Fig. 1.6. In the figure, the *LoadableDevice* is a child class of the *Device*. Therefore, the *ModemDevice* inherits all the attributes, such as *usageState* and *adminState*, and all the behaviors, such as *allocateCapacity* and *deallocateCapacity* from its parent class, *Device*. Moreover, the *LoadableDevice* has its private behaviors: *Load* and *Unload*. Detailed definitions of interfaces can be found in the SCA specification [2].

1.3 Hardware Platforms of Software Defined Radio Receiver

In the previous section, a brief overview of the software architecture used in developing an SDR receiver has been provided. Another important issue in the development of the SDR technology is the proper choice of hardware platforms on which the software architecture will be built. An appropriate choice will provide proper resources to the hardware objects defined in software without extra power consumption. Currently, most popular hardware platforms include DSP processors, Field Programmable Gate Arrays (FPGAs), and Application Specific Integrated Circuits (ASICs). This section will provide a brief discussion of the features and applications of different SDR hardware platforms.

1.3.1 Comparison of hardware platforms

The objectives in the SDR research involve the design of power-efficient processors and hardware architectures, in particular, for broadband communications. There are four key issues that must be properly considered when choosing hardware platforms: flexibility, modularity, scalability, and performance [1]. Flexibility means the ability to adapt to various air interface protocols. Modularity means that the radio system is highly sectored to facilitate the replacement and update of subsystems. Scalability is the ability to expand to larger systems without changing the architecture. The performance of a hardware platform is characterized by power consumption, computational ability, and cost. In this subsection, three hardware platforms (DSPs, FPGAs, and ASICs) will be briefly examined and compared.

DSP Processors Based Hardware Platform

A digital signal processing (DSP) processor can be viewed as a microprocessor optimized for digital signal processing applications. A DSP-based platform can be programmed by high level languages (HLL), such as C/C++, with the help of proper compilers. However, most DSPs can provide limited parallelism. Some parallel algorithms have to be broken into serial pieces to be executed in DSPs. Moreover, DSPs may not be optimal for some specific application as it might take more clock cycles to execute some instructions.

It is important to choose the right DSPs for a particular application with respect to its architecture, speed, multiprocessor capabilities, MAC units, instruction set, power consumption, and cost. For example, in the DS-CDMA/OFDM context, the efficiency of performing the Multiply-and-Accumulation (MAC) operation is a good performance indicator, because many radio functions are MAC intensive.

According to the Moore's law, processing power for the same volume and power consumption would be doubled every 18 months. Nowadays, most DSPs can operate in the gigahertz range. For example, Texas Instruments *C64X* DSPs family can provide 8800 million instructions per second (MIPS) at 1100 MHz! A UMTS transceiver baseband chip-rate load is 3724 MIPS. Therefore, DSPs can comfortably meet the baseband computational requirements of existing communication protocols.

However, computational requirements at RF and IF stages have usually exceeded the maximum capability of DSPs chips. To achieve a flexible and affordable hardware platform, DSPs should be assisted by FPGAs/ASICs-based accelerators.

Field Programmable Gate Array (FPGA) Based Hardware Platform

The chip-rate processing can be completed by high MIPS rated FPGA devices. However, a FPGA's function is static after boot-up. FPGAs must be switched to off-line in order to reprogram. This procedure usually takes fractions of a second. Pipeline and parallelism are two major advantages of FPGAs, which can significantly improve the efficiency of hardware. On the other hand, pipelining introduces a relatively large latency. This makes FPGAs not suitable for delay-sensitive applications (such as voice communication).

Functions of FPGAs can be described using hardware languages, such as VHDL and Verilog. Based on the VHDL description of algorithms, synthesis tools will decide the detailed hardware architecture. Therefore, the necessary hardware resources and maximum speed are decided based on both VHDL design and synthesis tools. This is another important difference from DSPs which can provide only fixed clock frequency. Two major suppliers of FPGAs are Xlinix and Altera. Both suppliers have the ability to provide very powerful FPGAs with millions of gates. The latest product information can be found on their respective official webpages.

Application Specific Integrated Circuits (ASICs) Based Hardware Platform

Application Specific Integrated Circuits (ASICs) are the most specialized hardware approach which heavily focuses on specific applications. ASICs are generally used when FPGAs/DSPs-based platform can not provide enough processing power, such as in the RF stage of the SDR receivers. However, the lack of flexibility prevents ASICs from being used in the baseband implementations of SDR receivers where flexibility is the priority.

A Brief Comparison of Hardware Platforms

In general, DSP cores are more suitable for the realization of complicated algorithms and control functions [10], while the dedicated hardware, such as ASICs and FPGAs, are usually used for computation-intensive functions, such as matched filtering and correlators, path searcher and FFT. The core digital signal processing hardware can be implemented through microprocessors, FPGAs, and/or ASICs. Basically, DSPs provides the maximum flexibility, but also the highest power consumption and lowest computational rate, whereas ASICs offer the minimal flexibility, but the lowest power consumption and highest computational rate. FPGAs, somehow, lie in between. The DSP-based platform with FPGA/ASIC accelerators is the most popular hardware platform where DSP processors execute most functions and FPGA/ASIC accelerators execute specified computation-intensive tasks [11]. In the next section, a DSP-based SDR receiver architecture operating in the DS-CDMA/OFDM composite radio environment will be proposed.

1.4 A SDR Radio Receiver in DS-CDMA/OFDM Composite Radio Environment

The convergence of different networks, which can complement each other to provide a full-coverage high-bandwidth network has become the future trend of wireless communications technologies. For example, wireless local area network (WLAN) is an ideal complementary network of the Universal Mobile Telecommunication System (UMTS) because of its small-coverage and high-bandwidth. The core technologies of UMTS and WLAN are Direct Sequence Code Division Multiple Access (DS-CDMA) and Orthogonal Frequency Division Multiplexing (OFDM), respectively. Therefore, a high-performance SDR receiver, which can operate in a DS-CDMA/OFDM composite radio environment is attractive.

In this section, the architecture of an SDR radio receiver will be proposed to provide high performance and flexibility in the DS-CDMA/OFDM context. Moreover, based on the receiver architecture, an in-depth study of a new highly-efficient estimation algorithm for both DS-CDMA and OFDM systems will be proposed in the following chapters.

1.4.1 Introduction to DS-CDMA and OFDM systems

DS-CDMA is the spread spectrum technology used for UMTS. The DSP-based implementation of DS-CDMA has been proven to be practical [1]. For components requiring the most computational capability, such as RF front-ends, they have to be implemented in ASICs. However, the control functions of the RF front-ends, such as automatic frequency control (AFC), automatic gain control (AGC), and frequency synchronizer, can be conducted in DSP cores. Moreover, some baseband processing

components, which require heavy computational capability, such as a Turbo decoder, are normally implemented in dedicated hardware. In a typical DS-CDMA receiver, *multipath searcher*, *Rake finger*, and *channel estimator* are the most important components, which also place enormous computational burden on the receiver [1].

The Orthogonal Frequency Division Multiplexing (OFDM) transmission divides a broadband channel into many parallel overlapping narrowband channels to minimize the complexity of equalization and achieve high spectral efficiency. The main principle of this transmission technique is to divide the available channel bandwidth in to various subchannels, and transmit data in parallel on all subchannels. This transforms a frequency selective fading channel into flat fading channels, which eases the equalization. However, even in a flat fading channel environment, an channel equalization module is required to compensate for the amplitude attenuation caused by wireless channels. In addition to simple channel equalizations, other techniques, such as cyclic prefix (CP), are also used in OFDM system to combat against the distortion from wireless channels.

In an OFDM receiver, the cyclic prefix is removed before the Fast Fourier Transform (FFT) demodulation. The time and frequency offset estimation is used to decide the FFT sample boundaries. After the removal of CP and decision of sample window, the FFT is executed within the sample window to demodulate the received signals. Pilot bits are extracted from demodulated symbols to estimate channel profiles. After channel equalization and symbol mapping, the received symbols are sent to deinterleaver, descrambler, Viterbi decoder, etc..

Detailed models of the CDMA and OFDM systems will be given in Chapter 2.

For a DSP-based SDR receiver, which demands large computational capability, reducing the computational requirements from these components is highly desired. Therefore, an important research issue on DSP-based SDR platforms is the develop-

ment of efficient algorithm [7]. In this thesis, based on the proposed SDR receiver architecture, we develop an efficient generic channel estimation and equalization algorithm. Detailed information can be found in Chapter 3.

1.4.2 The architecture of the proposed SDR receiver

Functionally, the structure of the proposed SDR receiver architecture operating in DS-CDMA/OFDM composite radio environment can be divided into 4 modules: *Correlation*, *Demodulation*, *Demapping*, and *Estimation*. Note that the time and frequency offset estimation function is included in the *Correlation* block. The functional blocks of the proposed SDR receiver architecture is shown in Fig. 1.7.

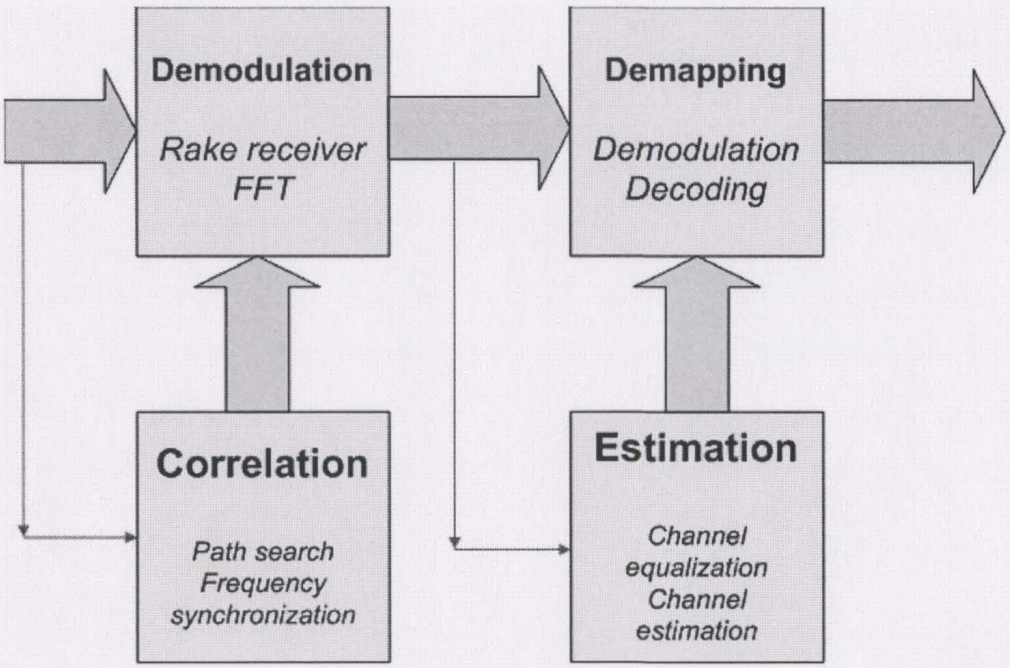

Figure 1.7: The functional blocks of baseband SDR receiver for DS-CDMA/OFDM composite radio environment.

Firstly, the received signal will be processed by the *Correlation* module to identify possible subpaths and time/frequency offsets. Then, the *Demodulation* module, which is configured by the information extracted by the *Correlation* module, will demodulate the received signal. Moreover, the *Estimation* module will estimate the wireless channel condition from the demodulated signal and compensate the distortion imposed by wireless channels using channel equalizers. Finally, the *Demapping* module will further process the received signal, which has been demodulated and compensated by this step.

The algorithms used in the *Correlation* and *Demapping* modules are very similar for both DS-CDMA and OFDM systems. However, in the *Demodulation* and *Estimation* modules, the traditional Rake receiver is used for DS-CDMA systems and the FFT demodulator is used for OFDM systems. There exist distinctive differences between them.

These four blocks can be mapped to four coprocessors and one core processor architecture. The communication between DSP processors is realized using function call and address passing. The architecture of the hardware platform of the proposed DS-CDMA/OFDM baseband SDR receiver follows a typical SDR receiver [3, 4], as shown in Fig. 1.8 .

1.5 Motivation

The research of innovative generic algorithms for the demodulation and estimation blocks is very challenging. Particularly, the traditional Rake receiver architecture for DS-CDMA systems is known as computationally burdensome and incompatible with the FFT-based receiver architecture for OFDM systems. To eliminate the necessity of Rake receivers, we have investigated the functionality of the Rake receiver and

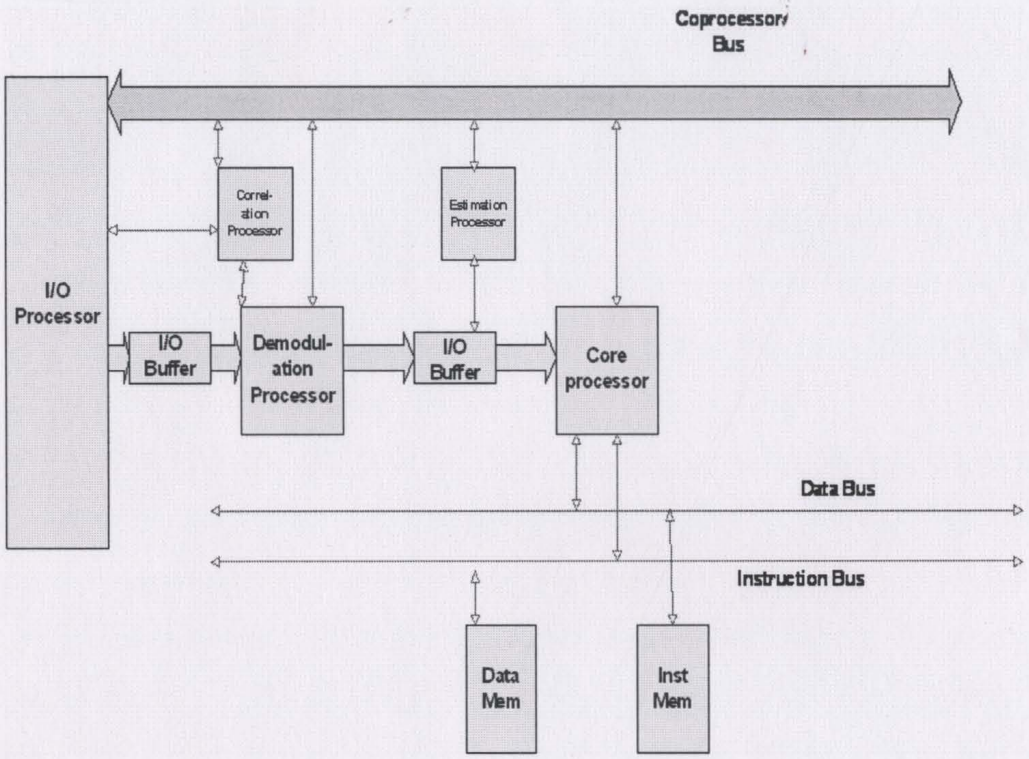

Figure 1.8: The hardware platform of the DSP-based baseband SDR receiver for DS-CDMA/OFDM composite radiofouts environment [3, 4].

found that the main tasks of the Rake receiver include the equalization of multipath fading channels and exploitation of the multipath diversity. Therefore, our goal is to come up with an efficient and low-cost channel estimation and equalization scheme to replace the traditional Rake receivers for DS-CDMA systems. The same module should also be used in the OFDM receiver architecture with some reconfiguration via software. in this way, a radio receiver in composite radio environment can be easily realized using SDR.

Frequency domain equalization (FDE) has been proven to be efficient in OFDM systems [12, 13, 14, 15]. Moreover, the FDE is a low-cost equalization scheme, which is very suitable for implementation using the SDR technology. Therefore, the main purpose of this thesis is to study a FDE-based generic equalization scheme, which is highly efficient for DS-CDMA/OFDM composite radio systems.

In order to work closely with the FDE, a frequency domain estimation algorithm is desired. In this thesis, we also proposed a generic frequency domain channel estimation algorithm, which can jointly estimate synchronization parameter and channel impulse response (CIR) in the frequency domain in DS-CDMA systems, and can jointly estimate the frequency offset and CIR in frequency domain in OFDM systems. Based on the expectation-maximization (EM) algorithm, this algorithm can fully satisfy the synchronization requirement for receivers in DS-CDMA systems. Therefore, the traditional Rake receiver is no longer necessary in the proposed SDR receiver architecture.

To further improve the performance of the proposed equalization scheme in DS-CDMA systems under fast fading channels, we propose an adaptive estimation scheme of Doppler shifts by utilizing the Basis Expansion Model (BEM). On the basis of accurate estimation of Doppler shifts, Doppler diversity can be exploited in DS-CDMA systems [16]. The simulation results show that, by incorporating the proposed esti-

mation algorithms, the performance of the FDE-based generic equalization scheme is satisfying in DS-CDMA/OFDM composite radio environment.

The rest of this thesis is organized as follows: Chapter 2 presents the signal and system models used in the analysis, including the DS-CDMA and OFDM system and channel models. A detailed discussion of the proposed generic frequency domain channel estimation and equalization scheme will be given in Chapter 3. Further discussion and analysis of the proposed receiver structure will be given in Chapter 4. Chapter 5 concludes the thesis and provides future research directions.

Chapter 2

System Modeling of Wireless Communications Systems

The International Telecommunications Union (ITU) initiated a plan to develop a single, worldwide and ubiquitous wireless communication standard in 2GHz range frequency band [17]. This plan, a.k.a., International Mobile Telephone 2000 (IMT-2000), has eventually led to the camps of 3G technology research community : CDMA2000 and Wideband CDMA (WCDMA).

CDMA2000 gives the evolution toward 3G from 2G CDMA sysems, which are based on IS-95A and IS-95B technologies. WCDMA, which is also called Universal

Air Interface	Mode of Operation	Duplexing Meth
CDMA2000	Multi-Carrier / Direct Spreading CDMA (DS-CDMA)	FDD
	Chip Rate $= N \times 1.2288 Mcps$, with $N = 1, 3, 6, 9, 12$	TDD
WCDMA	DS-CDMA,	FDD
	Chip Rate $= N \times 0.960 Mcps$, with $N = 4, 8, 16$	TDD

Table 2.1: Leading IMT-2000 Candiadate Standards as of 1998

Mobile Telecommunications Service (UMTS), is the evolution toward 3G from Global System for Mobile (GSM), IS-136, and Pacific Digital Cellular (PDC) systems. These two leading IMT-2000 candidate standards are shown and compared in Table 2.1 [17].

The key features of the CDMA2000 standard include:

1. Backward compatibility with IS-95A and IS-95B standard.
2. Downlink can be implemented using either multi-carrier or direct spreading.
3. Uplink can support a simultaneous combination of multi-carrier or direct spreading.
4. Auxiliary carriers to help with downlink channel estimation in forward link beamforming.

The key features of the WCDMA standard include:

1. Backward compatibility with GSM/DSC-1900 system.
2. Up to 2.048 Mbps on downlink in FDD mode.
3. Minimum forward channel bandwidth of 5 MHz.
4. Connection-dedicated pilot bits assist in downlink beamforming.

The features of the candidates for 3G technologies indicate that both CDMA2000 and WCDMA systems adopt DS-CDMA technology. Moreover, they both use auxiliary resources, such as auxiliary carriers in CDMA2000 systems and connection-dedicated pilot bits in WCDMA systems, to facilitate the operation of the system. In our research, a DS-CDMA system with pilot sequence is used for the study of 3G systems. This choice guarantees that our research has practical meanings and could be potentially incorporated into 3G communications systems in the future.

Along with the development of 3G cellular systems, Wireless Local Area Networks (WLANs) are also under tremendous developments. In addition to its original target of providing users to access wireless networks anytime and anywhere, WLAN could be used to provide the access for the last 100 meters into homes and businesses in competition with IMT-2000 [17]. Orthogonal Frequency Division Multiplexing (OFDM) has been explored for high speed data connections in the IEEE 802.11a standard to provide 54 Mbps WLAN connections. Moreover, OFDM has been considered as a very promising candidate for Beyond 3G technologies.

In this chapter, the basic concepts of CDMA and OFDM systems will be introduced. Because our focus is on the development of generic channel estimation and equalization algorithms for both systems, we will examine the channel models used in both CDMA and OFDM systems.

2.1 Wireless Communications Systems

In this section, we will briefly introduce the baseband models of DS-CDMA and OFDM systems. Moreover, the traditional receiver structures used in DS-CDMA and OFDM systems will be given.

2.1.1 Direct Sequence Code Division Multiple Access (DS-CDMA) System

Direct Sequence Code Division Multiple Access (DS-CDMA)-based systems utilize the spread spectrum signal to overcome the interference encountered in radio channels, such as jamming, Multiple Access Interference (MAI), and Inter-Symbol Interference (ISI) [18]. Moreover, the spread spectrum signal can be used in CDMA systems to

achieve message privacy. The block diagram of the baseband model of a typical DS-CDMA system is shown in Fig. 2.1 [19]. As shown in the figure, the *Spreading Code*

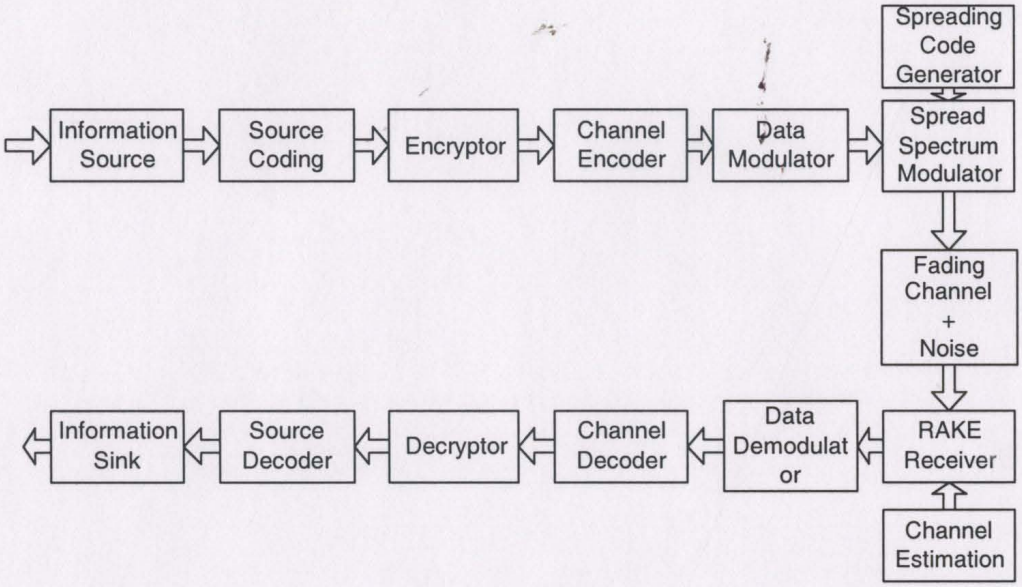

Figure 2.1: The block diagram of the baseband model of a typical DS-CDMA system

Generator generates the spreading code, which will be used to spread the frequency spectrum of the information-bearing signal. In a DS-CDMA system, the transmitted signal can be represented as

$$s(t) = \sum_{n=-\infty}^{\infty} a(n)P(t - nT), \tag{2.1}$$

where $P(t)$ is the pulse shaping waveform, $a(n)$ is the spread and scrambled symbol, and T denotes the length of duration of a symbol.

In DS-CDMA systems, the signal to be transmitted is processed in the time domain. After passing through a radio channel, the received signal can be expressed as

$$r(t) = s(t) \otimes h(t) + N_r, \tag{2.2}$$

where N_r is the additive white Gaussian noise (AWGN), and $h(t)$ is the multipath channel impulse response (CIR), which will be discussed in details in the following sections.

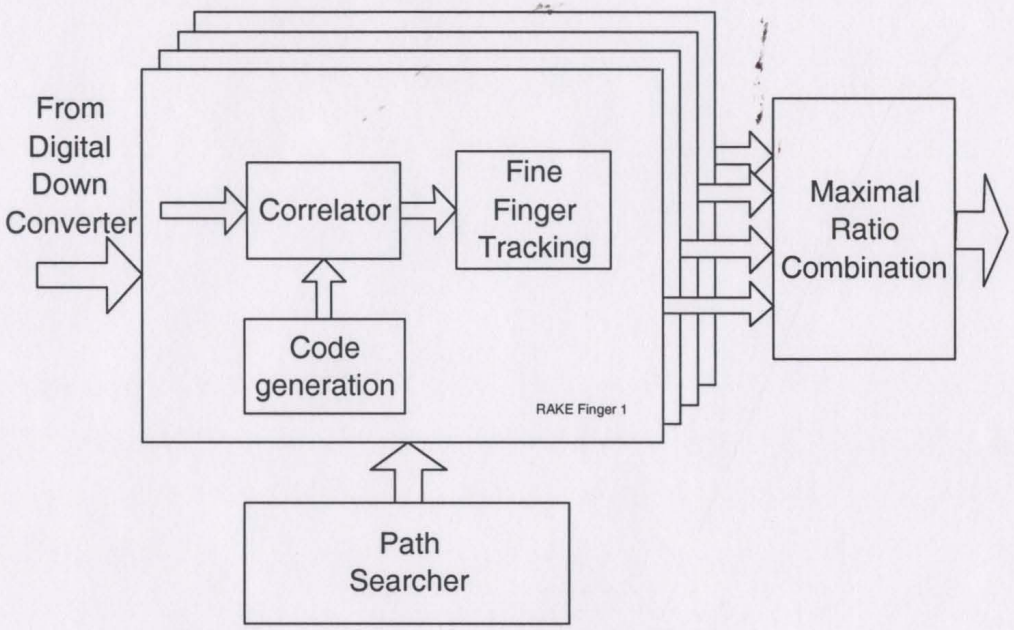

Figure 2.2: The block diagram of the Rake receiver [1].

The received signal will be sent to the Rake receiver to despread and descramble. A typical structure of a four-finger Rake receiver is shown in Fig. 2.2 [1]. There are four main components in a typical Rake receiver: Path Searcher, Correlator, Code Generation, and Maximal Ratio Combination. Firstly, the path searcher despeads the received pilot signal and correlates it with a known pilot sequence at different code offsets. The range of code offsets to be searched is set according to the allowed delay spread. Through path searching, strong multipath signals will appear as peaks. According to the code offsets and the number of significant peaks, the number of multipath and the corresponding delay can be estimated. Secondly, the estimated subpath delay information will be sent to the *Code Generation* module to generate

the descrambled and despread code at the corresponding code offsets. Then, the *Correlator* will despread and descramble the received signal using the generated code. Finally, the despreaded signal from all Rake fingers will be combined using maximum ratio combination.

The Rake receiver is computationally intensive because of the multiple searching process in the *Path Searcher* module. Moreover, the Rake receiver suffers from significant performance degradation in fast fading channels [16]. In addition, the structure of Rake receivers is significantly different from the receiver structure used in OFDM systems. Reuse of the same module would not be feasible for radio receivers in composite radio environment. This severely impedes the convergence of DS-CDMA/OFDM receiver via SDR technology. Therefore, a generic receiver architecture, which can substitute for the traditional Rake receiver and can achieve maximum similarity with the OFDM receiver is highly desired.

2.1.2 Orthogonal Frequency Division Multiplexing (OFDM) System

Orthogonal Frequency Division Multiplexing (OFDM) is a Frequency-division Multiplexing (FDM) modulation technique for transmitting large amount of digital data over a radio wave. In an OFDM system, the radio signal is split into multiple smaller sub-signals, which are then transmitted simultaneously on different frequencies. OFDM utilizes parallel data transmission and overlapping sub-carriers to fully utilize the bandwidth [12]. The baseband model of a typical OFDM system is shown in Fig. 2.3 [5].

Discrete Multitone Modulation (DMT) is used in OFDM systems to achieve parallel data transmission [20]. In DMT, the symbol sequence to be transmitted, $s(t)$,

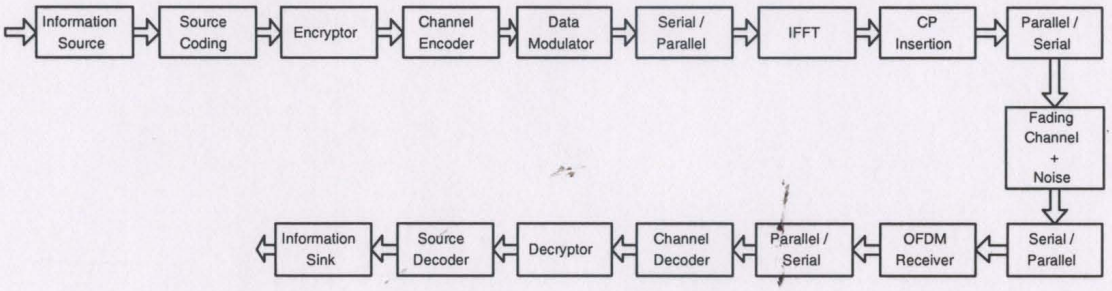

Figure 2.3: The baseband model of a typical OFDM system [5].

is obtained through a N-Point IFFT transform of the information sequence $\{a(n)\}$. Let $n = mN + k$, where $k = 0, 1, ..., N-1$ and m is an integer, we have

$$b(mN+k) = \frac{1}{N}\sum_{l=0}^{N-1} a(mN+l)e^{j2\pi kl/N}, k = 0, 1, ..., N-1 \tag{2.3}$$

where $b(mN+k)$ is the output of the N-Point IFFT of the information sequence $a(n)$. After passing $b(mN+k)$ through the "Parallel to Serial" module, The transmitted signal can be expressed as

$$s(t) = \sum_{n=-\infty}^{\infty} b(n)P(t-nT), \tag{2.4}$$

where $P(t)$ is the pulse shaping waveform. The transmitted signal $s(t)$ is actually defined in the frequency domain. Therefore, in a perfectly synchronized OFDM system, the transmitted signal can be viewed as passing through a set of parallel Gaussian channels [21]. This greatly facilitates the utilization of frequency domain equalization techniques in OFDM systems. However, at the receiver end, the received signal before the "FFT" module can still be modeled as

$$r(t) = s(t) \otimes h(t) + N_r, \tag{2.5}$$

where N_r is the AWGN signal, and $h(t)$ is the CIR of the multipath channel.

When $s(t)$ passes through a band limited multipath channel, inter symbol interference (ISI) will occur. In order to alleviate ISI in OFDM systems, two special

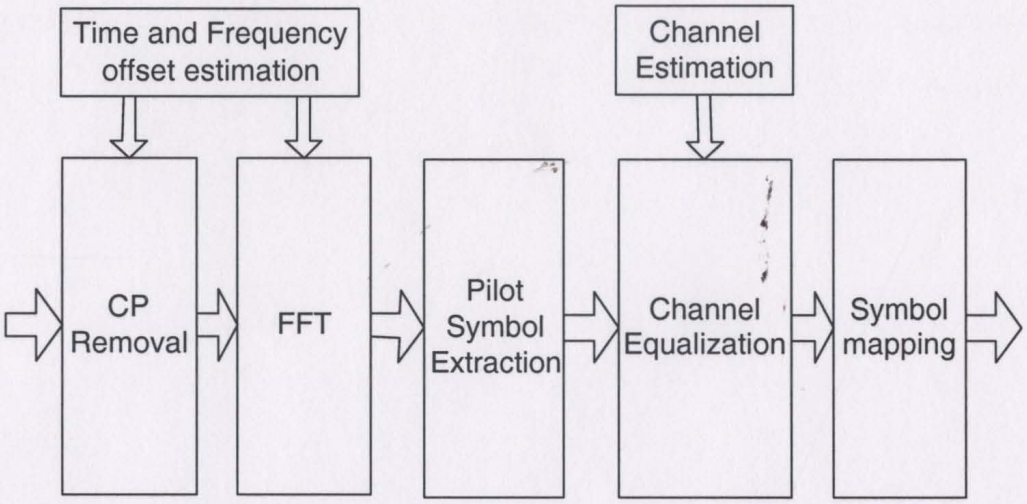

Figure 2.4: The block diagram of the baseband receiver in OFDM systems

methods are used: the virtual carriers method in which the zero-padding carriers are used in the roll-off region of the pulse shaping filter, and the guard interval method in which a cyclic extension of IFFT output blocks is inserted between successive information blocks. Both methods sacrifice bandwidth efficiency to gain more reliable communications.

Coded OFDM (COFDM) adopts powerful channel coding techniques to combat both multipath distortion and impulse noise at the cost of increased computational requirements and power consumption. Assuming that the total channel bandwidth is B and the number of carriers is N_c, the bandwidth of each sub-channel is B/N_c. Information transmitted through subchannels may experience deep fading, which greatly increases the need for proper channel coding.

Interleaving is another important technology to combat frequency selective fading channel. There are two types of interleaving in OFDM systems: bit-level interleaving and frequency interleaving. Bit-level interleaving is the same as in a single-carrier communications system. Frequency interleaving scatters sub-carriers among subchan-

nels to mitigate the frequency selective fading. Moreover, such division of subchannels also provides a form of frequency division multiple access (FDMA) [22].

Channel equalization plays an important role in compensating ISI caused by frequency selective fading channels. Time domain channel equalizer can not efficiently handle ISI [14], if the impulse response of a wireless channel is very long, which means the bandwidth of the wireless channel is relatively small compared to that of the transmitted signal [17]. In order to configure the channel equalizer, an accurate channel estimation algorithm is pivotal. The comb-type pilot insertion has been proved to be an efficient frequency domain channel estimation scheme in fast fading wireless channels [23].

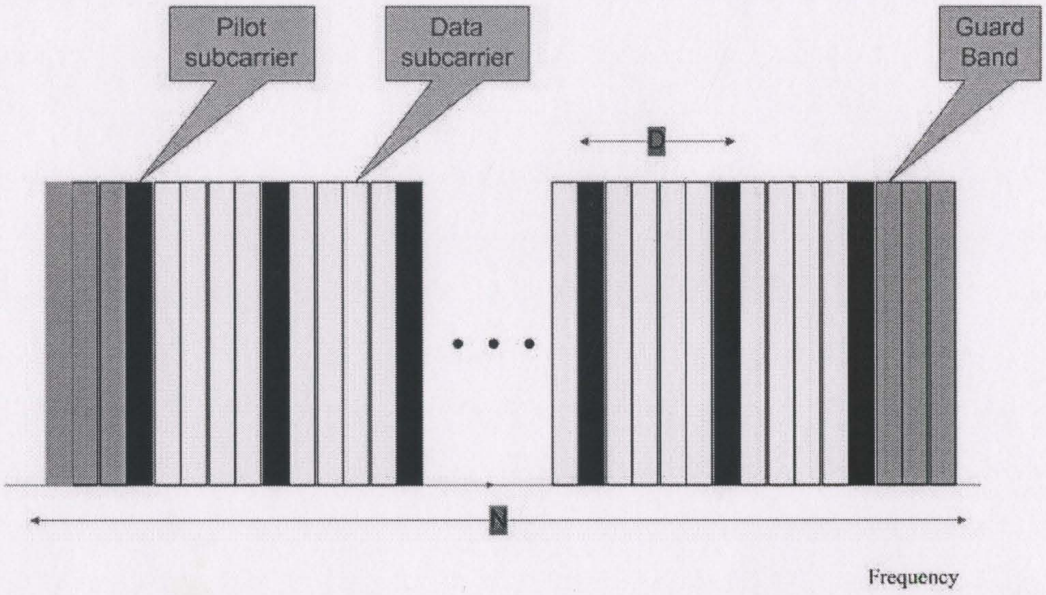

Figure 2.5: An illustration of the Comb Type Pilot Insertion Scheme

A typical comb-type pilot carrier insertion scheme is given in Fig. 2.5. In our research, the number of pilot carriers inserted is set as M, which is larger than the normalized maximum excess delay $\frac{\tau_{max}}{T}$, where τ_{max} is the maximum excess delay and

T is the symbol interval [24]. The spacing between pilot sub-carriers is $D = \frac{N}{M}$, where N is the total number of sub-carriers. The information of channel frequency response (CFR) can be easily extracted from these inserted known pilots [23].

OFDM system adopts a frequency domain equalizer, which is a simple one-tap multiplier bank under the assumption that the multipath delay is less than the guard interval [14]. Let us denote the channel transfer function as $H(\omega)$, and H_N^k stands for its k^{th} N-Point sample, according to minimum mean-square error (MMSE) criterion [18], the complex coefficient of the k^{th} multiplier is

$$c_k = \frac{H_k^*}{|H_k^2| + \sigma_n^2/\sigma_a^2}, \tag{2.6}$$

where σ_n^2 denotes the mean power of noise, and σ_a^2 is the mean power of signal. In [14], the feasibility of frequency domain equalization for both OFDM and DS-CDMA systems has been studied. As mentioned earlier, in software defined radio, one of the research objectives is to maximize the similarity of functionality between different systems. A highly efficient frequency-domain based channel equalization and estimation module is very attractive in SDR receiver design for composite radio applications. A channel estimation algorithm is used to extract and estimate the information of radio channel, while channel equalization is used to compensate for intersymbol interference (ISI) created by the bandlimited multipath radio channel. Therefore, a thorough understanding of the nature of the radio channel is very important. In the following section, we will discuss some important wireless channel models which we will use in our research. For the rest of this thesis, we will focus on the discussion of frequency domain estimation in DS-CDMA systems.

2.2 Channel Models

The wireless radio channel is the major factor limiting the performance of wireless communication systems. The effects of wireless radio channel include large-scale path loss, small-scale fading and multipath effects [18]. Large-scale path loss can be compensated by increasing transmission power. Small-scale fading and multipath effects are the result of ISI, which can be compensated by channel equalization. Therefore, a mathematical model, which could provide an accurate description of the multipath channel is important in the research of channel estimation and equalization algorithms. In this section, the mathematical model of the physical channel and the three most popular channel models (JAKES Model, Tapped Delay Line Model, and Basis Expansion Model) will be introduced. These channels models provide the foundation for our research.

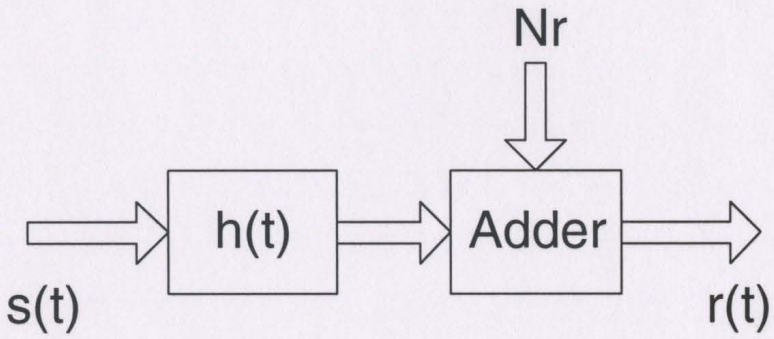

Figure 2.6: Generic Channel Model

As shown in Fig. 2.6, any channel model can be roughly divided into two parts: channel impulse response (CIR) and additive white gaussian noise (AWGN). The CIR, denoted by $h(t)$, depicts the multipath effects of the radio channel caused by reflection, diffraction, and scattering [17]. The noise signal, N_r, includes multiple access interference (MAI) as well as additive white gaussian noise (AWGN). Due to

the randomness of MAI, N_r can be approximated as AWGN [25, 26, 27]. Therefore, most of the channel models focus on the modelling of channel impulse response, $h(t)$.

2.2.1 Physical Channel Model

In most communications systems, the unpredictable changes in the time-varying impulse response (TVIR) of channel, $h(t;\tau)$, can be modeled as a stochastic process of time variable t, where τ denotes the time delay of different subpaths.

The discrete version of a physical channel impulse response can be modeled as

$$h[n;\nu] = \sum_{c=1}^{C} \psi(\nu T - \tau_c) \sum_{r=1}^{R} G_{c,r} e^{j2\pi n T f_{c,r}}, \tag{2.7}$$

where T denotes the symbol interval, $\psi(t)$ stands for the total impulse response of transmitting, receiving filter, and TV channel, τ_c is the delay of c^{th} cluster, $G_{c,r}$ and $f_{c,r}$ stand for the complex gain and the frequency offset of the r^{th} ray of the c^{th} cluster. Note that n and ν are the discrete sample of t and τ, respectively.

In this thesis, the wide-sense stationary uncorrelated channel (WSSUC) is assumed. WSSUC describes a channel using a wide-sense stationary process for each fixed delay τ. It is uncorrelated for different delays. WSSUC is a standard assumption to describe multipath wireless channels [28].

2.2.2 Jakes Model

The Jakes model is a deterministic channel model which is broadly used in the simulation of physical channel [29]. In our research, the modified Jakes model is used in the simulation platform.

Jakes model assumes that there are N equal-strength rays arriving at a moving object with uniformly distributed arrival angles α_n. However, the original Jakes

model, which was proposed in [29] to generate multiple uncorrelated waveforms, has the risk of producing highly correlated waveforms under certain circumstances [30]. Therefore, we adopt the modified Jakes model proposed in [30], which has been proven to be able to generate multiple uncorrelated waveforms more efficiently.

By utilizing orthogonal vectors, such as the Walsh-Hadamard (WH) codewords, the k^{th} waveform generated by the modified Jakes model can be expressed as

$$T(t,k) = \sqrt{\frac{2}{N_0}} \sum_{n=1}^{N_0} A_k(n)\{[cos(\beta_n) + jsin(\beta_n)]cos(\omega_n t + \theta_n)\}, \tag{2.8}$$

where

- n denotes the discrete time index;
- $N_0 = N_w/4$, where N_w is the number of rays;
- $A_k(n)$ is the k^{th} WH code sequence in n;
- $\beta_n = \pi n/N_0$;
- $\omega_n = \omega_M cos(\alpha_n)$, where $\omega_M = 2\pi f v/c$ is the maximum Doppler shift, v is the vehicle speed, f is the carrier frequency, and c is the speed of light;
- θ_n is randomly selected value from $[0, 2\pi]$.

We use $\alpha_n = \frac{2\pi(n-0.5)}{N_w}$ in our simulation. Moreover, N_0 is should be a power of 2 whose value should lie in $[12, 24]$ [30]. In our system, we choose $N_0 = 16$ to simulate a general situation.

2.2.3 Tapped-Delay Line Channel Model

In the tapped-delay line channel model, the channel impulse response can be expressed as

$$h(n) = \sum_{l=1}^{L} h_l(n)\delta(n - \left[\frac{\tau_l}{T}\right]) + N_r, \tag{2.9}$$

where

- $\left[\frac{\tau_l}{T}\right]$: calculate the nearest integer of $\frac{\tau_l}{T}$;
- τ_l : delay of the l^{th} subpath;
- T : Symbol interval;
- N_r: noise at the receiver end;
- $h_l(n)$: discrete complex channel coefficients of the l^{th} subpath;
- L : number of subpaths.

In equation (2.9), N_r includes multiple access interference (MAI) as well as additive white gaussian noise (AWGN). Due to the randomness of MAI, N_r can be approximated by AWGN [25, 26]. Moreover, in the analysis, we assume that the wireless channel represents a noisy version of the wide sense stationary uncorrelated scattering (WSSUS) process [18].

Although the tapped-delay line channel model has been broadly adopted in the analysis of wireless communications systems, it is a coarse approximation of the physical channel [31]. The main flaw of this channel model lies in that it is incapable of describing the frequency spread feature of fast fading channels. On the other hand, based on joint time-frequency representations (TFR's), basis expansion model has been to proven to be a better candidate, which can provide more accuracy in depicting the fast fading channel and exploiting Doppler diversity [16].

2.2.4 Basis Expansion Model (BEM)

The idea of a deterministic basis expansion model (BEM) lies in the fact that a Doppler-induced radio channel can be well approximated by superimposed sinusoids

with constant amplitudes and random phases [32]. In the basis expansion model, the channel impulse response is approximated as

$$h[n;\nu] \approx \sum_{l=1}^{L} \delta(\nu - \tau_l) \sum_{q=-Q}^{Q} h_{q,l} e^{j2\pi qn/N_{mod}} \tag{2.10}$$

where

- n denotes the discrete time index;
- ν denotes the discrete time delay of each subpath;
- l denotes the index of subpaths;
- L denotes the number of subpaths;
- $\delta(n)$ denotes the discrete impulse signal.

In equation (2.10), the time-varying (TV) channel is modeled as a superposition of TV bases (complex exponentials) and time-invariant (TI) coefficients, $h_{q,l}$. Each channel tap can be viewed as the sum of $2Q+1$ Doppler subpaths. Therefore, there are $L \times (2Q+1)$ subpaths in all. The method of determining the dimension of a channel, (L, Q), can be found in [33].

Equation (2.10) also shows that the Doppler spread of radio channel based on the BEM model is equal to $Q/(N_{mod}T_c)$. Moreover, because the BEM is periodic with a period of N_{mod} and the practical radio channel is not periodic, N_{mod} should be larger than the length of frame, denoted as N. In communications systems, *frame* is defined as a fixed block of data transmitted as a single entity. In this paper, we choose $Q = 1$. After Q is decided, we have $N_{mod} = \lceil Q/(T_c f_{max}) \rceil$, where f_{max} is the Doppler spread. However, f_{max} is often not available at the receiver. In this case, N_{mod} can be empirically set as $3N$ for approximation[31].

Using the BEM model, the received signal in a typical DS-CDMA system can be expressed as

$$r(n) = \sum_{l=1}^{L} \sum_{q=-Q}^{Q} h_{q,l} e^{j2\pi qn/N_{mod}} a(n - \tau_l) + N_r. \tag{2.11}$$

where

- n denotes the discrete time index;
- $a(n)$ denotes the transmitted signal;
- L denotes the number of subpaths;
- N_r denotes the AWGN in the system.

The BEM model is capable of describing TV channels with more accuracy. However, as shown in Equation 2.10, the values of Doppler shifts are deterministic and can not be modified according to varying channel conditions. This problem can be solved by our proposed adaptive estimation of Doppler shifts, which will be described in detail in the next section.

2.2.5 Summary

In this section, a brief review of the DS-CDMA system and the OFDM system has been provided. A complete communication system model has been established. Based on that, a detailed study of channel models has been conducted. These system models and channel models, including the physical model and mathematical models, provide a solid basis for the in-depth research of channel estimation and equalization algorithms in the following sections.

Chapter 3

Adaptive Channel Estimation and Equalization Scheme

3.1 Related Work

As the most promising candidates of the technologies used in next generation wireless networks, DS-CDMA and OFDM systems have received significant attention worldwide. In DS-CDMA and OFDM systems, highly-efficient channel estimation and equalization schemes play an important role in improving the performance of radio receivers. Channel estimation and equalization can be easily solved in slow fading channels with the help of pilot sequences. However, the corresponding schemes for fast fading channels remains challenging. In this chapter, we will focus on the development of highly-efficient frequency domain channel estimation and equalization to fight against fast fading effects in DS-CDMA systems.

A fast fading multipath channel is also referred to be a doubly selective channel because the channel impulse response (CIR) exhibits not only frequency-selectivity but also time-selectivity [31, 32, 34, 35]. Recently, diversity techniques have been

used in wideband radio receivers to combat fading effects of doubly selective channels [18]. In particular, Rake receivers have been widely used in DS-CDMA systems to achieve multipath diversity [18]. However, a traditional Rake receiver suffers from high computational complexity and limited ability of exploiting the inherent diversity nature of doubly selective channels. Moreover, it suffers from significant performance degradation in fast fading channels [16]. Therefore, to improve the performance of DS-CDMA radio receivers in fast fading channels, the inherent diversity of fast fading channels must be properly addressed.

As an attempt to exploit the inherent diversity of doubly selective channels, an innovative concept of Doppler diversity has been proposed [16]. The theoretical basis of Doppler diversity is the pseudorandom characteristic of Pseudo Noise (PN) codes used in DS-CDMA systems, which also ensures the orthogonality of different Doppler subpaths. The costly Rake receiver structure is used in [16] to exploit Doppler diversity in the receiver structure. However, estimation of Doppler shifts for different Doppler subpaths is not considered in their work. Therefore, in our research, two important aspects are addressed concerning a DS-CDMA receiver: a low-cost receiver architecture to efficiently exploit Doppler diversity, and algorithms for joint estimation of the synchronization parameter and CIR information which include Doppler shifts estimation.

As a low-cost approach to improve the performance of a DS-CDMA receiver, frequency domain equalization (FDE) has attracted significant research [36, 37, 38, 39, 40]. However, in those studies, complicated structures such as multiple-tap time-domain feedback filters are often assumed [36, 37], in which high computational complexity is associated. At the same time, although there are some efforts attempting to implement one-tap multiplier based FDEs in DS-CDMA receiver directly, either the work did not consider channel estimation [38], or only coarse channel estimation

algorithms are considered [39, 40]. It is highly desired that a highly-efficient channel estimation algorithm can be developed, which can work closely with the FDE to exploit Doppler diversity in a doubly selective channel to improve receiver performance.

A comprehensive understand of the nature of doubly selective channels is critical and necessary in developing channel estimation algorithms. The basis expansion model (BEM), in which the doubly selective channel is approximated by a number of complex exponentials, has been proven highly efficient and accurate [33]. In [31], a deterministic method is adopted to identify the parameters of the BEM model. However, the lack of a flexible estimation scheme makes it very difficult to adaptively adjust parameters of the BEM model according to the varying radio channel conditions, such as velocity changes. More detailed discussion on the BEM model has been given in Chapter 2.

In this chapter, by utilizing the BEM model, we propose an adaptive algorithm which can accurately estimate Doppler shifts for different Doppler subpaths in real-time applications. Based on the estimation of the Doppler shifts, an innovative FDE-based receiver architecture is proposed to exploit the Doppler diversity in fast fading channels in DS-CDMA systems. Moreover, we propose a frequency-domain joint estimation algorithm. In addition to an accurate estimation of the channel impulse response, we demonstrate that this estimation algorithm can also be used to obtain the synchronization parameter required in a DS-CDMA system. Such joint estimation of the synchronization parameter and CIR facilitates later equalization processing in a DS-CDMA receiver. Therefore, the traditional costly Rake receiver is not required. Another advantage of this joint estimation algorithm is that it can also be used in the OFDM system for the joint estimation of frequency offset and CIR. This feature enables a generic channel estimation and equalization module for receivers used in both DS-CDMA and OFDM systems.

With a common module of channel estimation and equalization, a generic structure of the receiver in the DS-CDMA/OFDM composite radio environment is proposed. The proposed FDE-based receiver structure has been proven to be efficient in both DS-CDMA and OFDM systems. Simulation results, which will be present in detail in Chapter 4, indicate that, with the help of the proposed adaptive estimation algorithm, the FDE-based receiver structure, which effectively exploits Doppler diversity, possesses outstanding performance in doubly selective channels. Therefore, this FDE-based receiver structure has great potential of being adopted in a SDR receiver working in DS-CDMA/OFDM composite radio environment.

The rest of this chapter is organized as follows: Section 3.2 presents channel estimation algorithms for slow fading channels in both DS-CDMA and OFDM systems. The proposed adaptive estimation scheme of Doppler shifts for different Doppler subpaths via BEM model in DS-CDMA systems will be given in Section 3.3. An EM algorithm-based joint estimation of the synchronization parameter and CIR in frequency domain will be given in Section 3.4. Based on the proposed frequency domain estimation, an FDE-based receiver structure working in DS-CDMA/OFDM composite radio environment will be given in Section 3.5.

3.2 Channel Estimation in Slow Fading Channels

A slow fading channel can be viewed as a time-invariant channel within a period of several frames. Moreover, a slow fading channel can be efficiently modeled by the tapped-delay line channel model described in equation (2.9), which is rewritten as

$$h(n) = \sum_{l=1}^{L} h_l \delta(n - \left[\frac{\tau_l}{T_c}\right]) + N_r. \tag{3.1}$$

Note that in equation (3.1), the time-invariant coefficients, h_l, substitute the time

variant coefficients, $h_l(n)$, which appear in the general form of a tapped-delay line channel model.

Under slow fading channels, the channel estimation can be achieved by exploiting the correlation of the channel impulse response at different times in DS-CDMA systems, while in OFDM systems, the channel estimation can be achieved by exploiting the correlation of channel frequency response at different frequencies. In the following subsections, we will briefly discuss the channel estimation algorithms used in DS-CDMA and OFDM systems in slow fading channels.

3.2.1 Channel Estimation in DS-CDMA Systems

In a typical DS-CDMA system, by utilizing the PN codes, the CIR information can be obtained from the received signal, which will be used to configure the Rake receiver to mitigate the intersymbol interference (ISI) [41]. In this section, the same idea is utilized: using PN codes, the channel information hidden behind the received signal will be extracted to facilitate the estimation of the CIR.

In DS-CDMA systems, the pilot sequence can be used for the equalizer to adapt to the mobile handset receiver. Under the tapped-delay line channel model given by equation(3.1), the received pilot signal can be expressed as

$$r(n) = \sum_{l=1}^{L} h_l a(n - \left[\frac{\tau_l}{T_c}\right]) + N_r, \tag{3.2}$$

where

- $[\ ]$: the nearest integer of $\frac{\tau_l}{T_c}$;
- $r(n)$: received signal at discrete time n;
- $a(n)$: transmitted pilot signal after scrambling and spreading;

- τ_l : delay of the l^{th} subpath;
- T_c : chip period ;
- h_l : discrete complex channel coefficients of the l^{th} subpath;
- L : the number of subpaths.

Note that h_l contains the transmit pulse shape $P(t)$, therefore, compared with equation (2.1), there is no $P(t)$ appearing in equation (3.2). Based on the prior knowledge of the pilot sequence, the output of a complex autocorrelation can be expressed as

$$\begin{aligned} \mathbf{E}\{y(m)\} &= \mathbf{E}\{\frac{1}{W}\sum_{n=1}^{W} r(n+m)a^*(n)\} \\ &= \mathbf{E}\{\frac{1}{W}\sum_{n=1}^{W}\sum_{l=1}^{L} h_l a(n+m-\left[\frac{\tau_l}{T_c}\right])a^*(n)\} + \mathbf{E}\{N_r\}, \end{aligned} \tag{3.3}$$

where $m = 0, 1, 2, \ldots, M$, and W is the chosen autocorrelation window size and M is the length of autocorrelation operation. Based on the pseudo-orthogonality of $a(n)$, equation (3.3) can be reduced to

$$\begin{aligned} \mathbf{E}\{y(m)\} &= \mathbf{E}\{\frac{1}{W}\sum_{n=1}^{W}\sum_{l=1}^{L} h_l \delta(m-\left[\frac{\tau_l}{T_c}\right])\} + \mathbf{E}\{N_r\}, \\ &\approx \frac{1}{W}\sum_{n=1}^{W}\sum_{l=1}^{L} h_l \delta(m-\left[\frac{\tau_l}{T_c}\right]), \end{aligned} \tag{3.4}$$

where $\delta(n)$ denotes the discrete impulse signal. During the above simplification, the assumptions that $\mathbf{E}\{a(n)a^*(n+m)\} = 0$, when $m \neq 0$ and $|a(n)| = 1$ and $\mathbf{E}\{N_r\} = 0$ are used. Assuming the number of the multipaths which can be detected is L_c, we have

$$\mathbf{E}\{y(\frac{\tau_i}{T_c})\} = \frac{1}{W}\sum_{n=1}^{W} h_i \approx h_i, \tag{3.5}$$

where $i = 1, 2, \ldots, L_c$. Equation(3.5) gives the average channel coefficients of the corresponding L_c detectable subpaths. Therefore, the estimated channel impulse response can be expressed as

$$\begin{aligned} \widehat{h}(n) &= \sum_{l=1}^{L_c} h_l \cdot \delta(n - \left[\frac{\tau_i}{T_c}\right]), \\ &\approx \sum_{l=1}^{L_c} \mathbf{E}\{y(n)\} \cdot \delta(n - \left[\frac{\tau_i}{T_c}\right]). \end{aligned} \tag{3.6}$$

Only when $n = \left[\frac{\tau_i}{T_c}\right]$, where $i = 1, 2, \ldots, L_c$, $\widehat{h}(n)$ can have nonzero value. For all other n values, $\widehat{h}(n)$ will be set to be zero, where $0 < n < M$.

The above zero-padding procedure will introduce some inaccuracy into the estimation of CIR. However, since the main subpaths of the wireless channel have been preserved, the interpolation inaccuracy of slow fading channels is limited. Nevertheless, in order to mitigate this inaccuracy, further adaptive process of $\widehat{h}(n)$ is necessary.

3.2.2 Channel Estimation in OFDM Systems

The pilot-based frequency domain (FD) channel estimations have been broadly studied in OFDM systems. Recently, a comb-type pilot insertion has been proved to be an efficient frequency domain channel estimation scheme [23],[24]. In our research, we simply adopt this scheme in our FDE-based generic receiver structure.

A brief illustration of the comb-type pilot insertion scheme in OFDM systems has been given in Section 2.1. Based on the same assumptions, M frequency samples of the inserted pilot carriers can be easily obtained through the correlation of the channel frequency response (CFR) at corresponding frequencies [24]. Assuming that the estimated M samples of CFR are $H_{m \cdot D}$, where $-\frac{M}{2} + 1 < m < \frac{M}{2}$, and D is the

pilot sub-carrier spacing, the complete estimation of CFR, $\widehat{H}_k$, can be given by

$$\widehat{H}_k = \sum_{m=-\frac{M}{2}+1}^{\frac{M}{2}} H_{m \cdot D} \cdot W_{k-mD,RC}, \tag{3.7}$$

where $H_{m \cdot D}$ is the CFR for the m^{th} pilot sub-carrier, $W_{k-mD,RC}$ are the frequency domain interpolation coefficients, which can be obtained according to various interpolation schemes. k is the index of discrete frequency.

Compared with traditional interpolation schemes, such as linear interpolation, and quadric interpolation, $W_{k-mD,RC}$ can provide the most accurate estimation when using a Raised-Cosine (RC) interpolation function given as

$$W_{l,RC} = \frac{sin(\pi Ml/N)}{\pi Ml/N} \cdot \frac{cos(\pi \beta Ml/N)}{d} 1 - 4\beta^2 (Ml/N)^2 \cdot e^{-j2\pi dl/N}, \tag{3.8}$$

where β is the roll-off factor of chosen function, and d is decided by the characteristics of the wireless channel [42].

The above interpolation-based frequency domain estimation is efficient in slow fading channels where the CFR can be viewed as time invariant. However, in fast fading channels, the performance of OFDM systems is degraded due to the frequency offset caused by the time selectivity of wireless channels. Numerous algorithms have been proposed to solve this problem. Among those algorithms, the Expectation-Maximization (EM) algorithm is getting popular because of its simplicity and high performance. In [43], an EM algorithm based joint estimation of frequency offset and channel impulse response is proposed. This joint estimation scheme can properly solve the problem of channel estimation for fast fading channels in OFDM systems. However, the estimation for doubly selective channels in DS-CDMA systems still needs to be addressed, especially in fast fading channels where $h_l(n) \neq h_l$ for different delay taps. In that case, the correlation procedure will introduce significant estimation inaccuracy and performance degradation. Therefore, the estimation for slow fading

channels in DS-CDMA systems can not be readily adopted when used in the fast fading channels.

Under fast fading channels, to accurately estimate the time-varying CIR, an adaptive channel estimation is desired. We noticed that the EM-based estimation algorithm is not exclusive for OFDM systems. This joint estimation of frequency offset and CIR in OFDM systems can be readily immigrated to DS-CDMA systems for the joint estimation of the synchronization parameter and CIR. Details will be given in Section 3.4.

In addition to a joint estimation of the synchronization parameter and CIR, an adaptive estimation of the Doppler shifts caused by fast fading channels is also proposed to facilitate the exploitation of the Doppler diversity, which is an unique feature of DS-CDMA systems. Detailed discussion will be given in the next section.

3.3 BEM Model and Doppler Diversity Techniques for Frequency Domain Channel Estimation in DS-CDMA systems

In this section, we propose an adaptive method of estimating the Doppler shift for each Doppler subpath. The method is based on the Expectation-Maximization (EM) algorithm. The proposed estimation method can provide subsequent modules in a receiver architecture, particularly, the frequency domain equalizer, with better estimation of Doppler shifts so that Doppler diversity can be exploited in more efficient way. In our discussion, we consider the scenario where $L = 4$ and $Q = 1$ in equation (3.9), where L stands for the number of total time domain channel subpaths and $2 \times Q + 1$ denotes the number of Doppler subpaths. It is easy to extend the results

to other scenarios.

3.3.1 Estimation of Time Invariant Coefficients

Using the BEM model, the received signal in a typical DS-CDMA system can be expressed as

$$r(n) = \sum_{l=1}^{L} \sum_{q=-Q}^{Q} h_{q,l} e^{j2\pi qn/N_{mod}} a(n-\tau_l) + N_r. \tag{3.9}$$

The detailed definition of coefficients used in equation (3.9) can be found in Section 2.2. To obtain the channel information, the time-shifted version of the received signal $r(n)$ is correlated with the known pilot signal $a(n)$ in a DS-CDMA system. The result is shown in equation (3.10), where the width of the correlation window is W and the length of shift is m.

$$\begin{aligned} \mathbf{E}\{y(m)\} &= \mathbf{E}\{\frac{1}{W}\sum_{n=1}^{W} r(n+m)a^*(n)\} + \mathbf{E}\{N_r\} \\ &= \mathbf{E}\{\frac{1}{W}\sum_{n=1}^{W}\sum_{l=1}^{L}\sum_{q=-Q}^{Q} h_{q,l} e^{j\frac{2\pi q(n+m)}{N_{mod}}} a(n+m-\tau_l)a^*(n)\} + \mathbf{E}\{N_r\} \end{aligned} \tag{3.10}$$

Considering the first subpath, where $l = 1$, assuming that $m = \tau_1$, $Q = 1$, and $|a(n)| = 1$, by applying the pseudorandom feature of $a(n)$, that is, $\mathbf{E}\{a(n+m)a^*(n)\} \approx 0$ when $m \neq 0$, equation (3.10) becomes

$$\mathbf{E}\{y(\tau_1, W)\} \approx \mathbf{E}\{\frac{1}{W}\sum_{n=1}^{W}\sum_{q=-1}^{1} h_{q,1} e^{j2\pi q(n+\tau_1)/N_{mod}}\} + \mathbf{E}\{N_r\} \tag{3.11}$$

We choose $2 \times Q + 1 = 3$ different values for the correlation window size, denoted by $\{W_1, W_2, W_3\}$. Using similar processing for each correlation window size, we have

$$\mathbf{E}\{\overline{\mathbf{y}}_{l=1}\} = \mathbf{E}\{\overline{\mathbf{C}}_{l=1}\} * \mathbf{E}\{\overline{\mathbf{h}}_{l=1}\} + \mathbf{E}\{\overline{\mathbf{N_r}}\}, \tag{3.12}$$

where

$$\overline{\mathbf{y}}_{l=1} = [y(\tau_1, W_1), y(\tau_1, W_2), y(\tau_1, W_3)]^T,$$

$$\overline{\mathbf{h}}_{l=1} = [h_{-1,1}, h_{0,1}, h_{1,1}]^T.$$

Each element of $\overline{\mathbf{C}}_{l=1}$ is given by $\frac{1}{W_x}\sum_{n=1}^{W_x} e^{j2\pi(n+\tau_1)(y-2)/N_{mod}}$, where $1 \leq x \leq 2Q+1$ and $1 \leq y \leq 2Q+1$. $\overline{\mathbf{N_r}}$ denotes the noise vector whose elements are Gaussian distributed random variables, which are independent of the transmitted signals and the wireless channels and have the expectation matrix $\mathbf{E}\{\overline{\mathbf{N_r}}\} = \overline{\mathbf{0}}$. Vector $\overline{\mathbf{y}}_{l=1}$ can be obtained using equation (3.11) according to the chosen $\{W_1, W_2, W_3\}$. Then, the estimation of the time-invariant vector of the first subpath, $\overline{\mathbf{h}}_{l=1}$, can be obtained by solving the resulting linear equations, which is given by

$$\mathbf{E}\{\overline{\mathbf{h}}_{l=1}\} = \frac{\mathbf{E}\{\overline{\mathbf{y}}_{l=1}\}}{\mathbf{E}\{\overline{\mathbf{C}}_{l=1}\}}. \tag{3.13}$$

Following a similar approach, other values of the time-invariant coefficient matrix of the doubly selective channel can be estimated. Assume that the number of significant subpaths is 4 ($L = 4$), the time-invariant coefficient matrix is given by

$$\overline{\mathbf{H}}_{BEM} = \begin{bmatrix} h_{-1,1} & h_{0,1} & h_{1,1} \\ h_{-1,2} & h_{0,2} & h_{1,2} \\ h_{-1,3} & h_{0,3} & h_{1,3} \\ h_{-1,4} & h_{0,4} & h_{1,4} \end{bmatrix}. \tag{3.14}$$

3.3.2 Estimation of Doppler Shifts

In this subsection, an adaptive estimation of the time-varying bases is proposed. With both the time-varying and the time-invariant information of the doubly selective channel available, a complete description of fast fading wireless channels can be eventually established.

Assume that $\frac{N}{P} = X$, where X is an integer greater than one, and N is the length of the transmitted data frame. Each frame of length N can be divided into X

subframes of length P. The following discussions will focus on each subframe. After all X subframes are equalized, they will be joined together to form the original frame of length N.

Under the BEM model, the received signal $r(n)$ is given by equation (3.9). The Discrete Fourier Transform (DFT) of $r(n)$ can be expressed as

$$\begin{aligned} R(k) &= \sum_{n=0}^{P-1} r(n)e^{-j2\pi nk/P} \\ &= \sum_{n=0}^{P-1}\sum_{l=1}^{L}\sum_{q=-Q}^{Q} h_{q,l}a(n-\tau_l)e^{-\frac{j2\pi n}{P}(k-\frac{qP}{N_{mod}}+f_e)}, \end{aligned}$$

where f_e denotes the unknown estimation error due to the Doppler shift. On the other hand, the Fourier Transform of the real received signal $\tilde{r}(n)$ can be approximated as

$$\begin{aligned} \tilde{R}(k) &= \sum_{n=0}^{P-1} \tilde{r}(n)e^{-j2\pi nk/P} \\ &= \sum_{n=0}^{P-1}\sum_{l=1}^{L}\sum_{q=-Q}^{Q} \tilde{h}_{q,l}a(n-\tau_l)e^{-\frac{j2\pi n}{P}(k+f_e(q))}, \end{aligned}$$

where $\tilde{h}_{q,l}$ are the real time-invariant coefficients of the doubly selective channel. $f_e(q)$ is the real Doppler shift of each Doppler subpath, where $q \in \{-1, 0, 1\}$. Subpath delay τ_l can be obtained during the estimation of the time-invariant coefficients. Moreover, during the estimation of Doppler shifts, we assume that $\tilde{h}_{q,l}$ is equal to the corresponding element in $\overline{\mathbf{H}}_{BEM}$ given in equation (3.14). The expectation of the correlation between $R(k)$ and $\tilde{R}(k)$ is shown in equation (3.15). To simplify the equation, we assume that $\mathbf{E}[a^*(n-\tau_{l_1})a(n-\tau_{l_2})] \approx 0$, where $\tau_{l_1} \neq \tau_{l_2}$. In addition, using Maclaurin Series expansion, we have $e^{\frac{-j2\pi f_e n}{P}} \approx 1 - j\frac{2\pi f_e}{P}n + \frac{1}{2}\left(j\frac{2\pi f_e}{P}n\right)^2$. Thus, the exponential parts of equation (3.15) can be approximated by its quadratic format. The real part of the correlation of $R(k)$ and $\tilde{R}(k)$ can be approximated by a quadratic form as

$$\Re\{\mathbf{E}[R^*(k)\tilde{R}(k)]\} \approx A(f_e)^2 + Bf_e + C, \tag{3.16}$$

$$
\begin{aligned}
\mathbf{E}[R^*(k)\tilde{R}(k)] &= \mathbf{E}[\sum_{n=0}^{P-1}\sum_{l_1=1}^{L}\sum_{q_1=-Q}^{Q}\sum_{l_2=1}^{L}\sum_{q_2=-Q}^{Q}\tilde{h}_{q_2,l_2}h^*_{q_1,l_1}a^*(n-\tau_{l_1})a(n-\tau_{l_2})e^{\frac{j2\pi n}{P}(f_e-\frac{q_1P}{N_{mod}}-f_e} \\
&\approx \frac{1}{P}\sum_{k=0}^{P-1}\{\sum_{n=0}^{P-1}\sum_{l_1=l_2=1}^{L}\sum_{q_1=-Q}^{Q}\tilde{h}_{-1,l_2}h^*_{q_1,l_1}\mathbf{E}[a^*(n-\tau_{l_1})a(n-\tau_{l_2})]e^{\frac{j2\pi n}{P}(f_e-\frac{q_1P}{N_{mod}}-} \\
&+ \sum_{n=0}^{P-1}\sum_{l_1=l_2=1}^{L}\sum_{q_1=-Q}^{Q}\tilde{h}_{0,l_2}h^*_{q_1,l_1}\mathbf{E}[a^*(n-\tau_{l_1})a(n-\tau_{l_2})]e^{\frac{j2\pi n}{P}(f_e-\frac{q_1P}{N_{mod}}-f_e(0))} \\
&+ \sum_{n=0}^{P-1}\sum_{l_1=l_2=1}^{L}\sum_{q_1=-Q}^{Q}\tilde{h}_{1,l_2}h^*_{q_1,l_1}\mathbf{E}[a^*(n-\tau_{l_1})a(n-\tau_{l_2})]e^{\frac{j2\pi n}{P}(f_e-\frac{q_1P}{N_{mod}}-f_e(1))}\} \\
&+ \mathbf{E}\{N_r\}. \\
&= \frac{1}{P}\sum_{k=0}^{P-1}\{\sum_{l=0}^{L}\tilde{h}_{-1,l}h^*_{-1,l}\sum_{n=0}^{P-1}e^{\frac{j2\pi n}{P}(f_e-\frac{-P}{N_{mod}}-f_e(-1))}+\sum_{l=0}^{L}\tilde{h}_{-1,l}h^*_{0,l}\sum_{n=0}^{P-1}e^{\frac{j2\pi n}{P}(f_e-f} \\
&+ \sum_{l=0}^{L}\tilde{h}_{-1,l}h^*_{1,l}\sum_{n=0}^{P-1}e^{\frac{j2\pi n}{P}(f_e-\frac{P}{N_{mod}}-f_e(-1))}+\sum_{l=0}^{L}\tilde{h}_{0,l}h^*_{-1,l}\sum_{n=0}^{P-1}e^{\frac{j2\pi n}{P}(f_e-\frac{-P}{N_{mod}}-f_e(0)} \\
&+ \sum_{l=0}^{L}\tilde{h}_{0,l}h^*_{0,l}\sum_{n=0}^{P-1}e^{\frac{j2\pi n}{P}(f_e-f_e(0))}+\sum_{l=0}^{L}\tilde{h}_{0,l}h^*_{1,l}\sum_{n=0}^{P-1}e^{\frac{j2\pi n}{P}(f_e-\frac{P}{N_{mod}}-f_e(0))} \\
&+ \sum_{l=0}^{L}\tilde{h}_{1,l}h^*_{-1,l}\sum_{n=0}^{P-1}e^{\frac{j2\pi n}{P}(f_e-\frac{-P}{N_{mod}}-f_e(1))}+\sum_{l=0}^{L}\tilde{h}_{1,l}h^*_{0,l}\sum_{n=0}^{P-1}e^{\frac{j2\pi n}{P}(f_e-f_e(1))} \\
&+ \sum_{l=0}^{L}\tilde{h}_{1,l}h^*_{1,l}\sum_{n=0}^{P-1}e^{\frac{j2\pi n}{P}(f_e-\frac{P}{N_{mod}}-f_e(1))}\}+N_r.
\end{aligned}
$$

where coefficients A and B are given by

$$
A = -\Re\{\sum_{l=1}^{L}\sum_{q_1=-1}^{1}\sum_{q_2=-1}^{1}\tilde{h}_{q_1,l}h^*_{q_2,l}\}\sum_{n=0}^{P-1}\frac{2\pi^2n^2}{P^2},
$$

$$
\begin{aligned}
B &= \Re\{\sum_{l=1}^{L}\sum_{q=-1}^{1}\tilde{h}_{-1,l}h^*_{q,l}\}\sum_{n=0}^{P-1}\frac{4\pi^2n^2}{P^2}f_e(-1) \\
&+ \Re\{\sum_{l=1}^{L}\sum_{q=-1}^{1}\tilde{h}_{0,l}h^*_{q,l}\}\sum_{n=0}^{P-1}\frac{4\pi^2n^2}{P^2}f_e(0)
\end{aligned}
$$

$$
\begin{aligned}
&+ \Re\{\sum_{l=1}^{L}\sum_{q=-1}^{1}\tilde{h}_{1,l}h_{q,l}^{*}\}\sum_{n=0}^{P-1}\frac{4\pi^2n^2}{P^2}f_e(1) \\
&+ \Re\{\sum_{l=1}^{L}\sum_{q_1=-1}^{1}\sum_{q_2=-1}^{1}\tilde{h}_{q_2,l}h_{q_1,l}^{*}\frac{qP}{N_{mod}}\}\sum_{n=0}^{P-1}\frac{4\pi^2n^2}{P^2} \\
&- \Im\{\sum_{l=1}^{L}\sum_{q_1=-1}^{1}\sum_{q_2=-1}^{1}\tilde{h}_{q_2,l}h_{q_1,l}^{*}\}\sum_{n=0}^{P-1}\frac{2\pi n}{P}. \\
&= B_1f_e(-1)+B_2f_e(0)+B_3f_e(1)+B_4, \qquad (3.17)
\end{aligned}
$$

The expression for constant C is not given because constant C will not affect the remaining processing. For the original received signal, by searching, we can get the value of f_e, noted as f_{e1}, which enables equation (3.16) to reach its maximum value. In addition, as A will have a non-zero value, it is well known that when $f_e = -\frac{B}{2A}$, equation (3.16) will have the maximum value. Therefore, we have

$$-\frac{B}{2A} = -\frac{B_1}{2A}f_e(-1) - \frac{B_2}{2A}f_e(0) - \frac{B_3}{2A}f_e(1) - \frac{B_4}{2A} = f_{e1} \qquad (3.18)$$

Following a similar procedure, through circularly shifting the columns of $\overline{\mathbf{H}}_{BEM}$ to the left, we obtain different estimations of received signal $r(n)$, which can be used to construct other linear equations, and we have

$$
\begin{aligned}
-\frac{B_2}{2A}f_e(-1) - \frac{B_3}{2A}f_e(0) - \frac{B_1}{2A}f_e(1) - \frac{B_4}{2A} &= f_{e2} \qquad (3.19)\\
-\frac{B_3}{2A}f_e(-1) - \frac{B_2}{2A}f_e(0) - \frac{B_1}{2A}f_e(1) - \frac{B_4}{2A} &= f_{e3} \qquad (3.20)
\end{aligned}
$$

Similarly, in equation (3.19) and equation (3.20), the shifted version of the $\overline{\mathbf{H}}_{BEM}$ is used, f_{e2} and f_{e3} are the corresponding searched values to achieve maximum correlation.

By solving the three linear equations given above, the estimation of Doppler shifts, $\{f_e(-1), f_e(0), f_e(1)\}$, can be obtained. In the above analysis, a scenario where three Doppler subpaths ($Q = 1$) is considered. However, this method can be easily extended to estimate Doppler shifts of arbitrary number of Doppler subpaths.

3.4 Joint Estimation of Synchronization Parameter and Channel Impulse Response

In the foregoing sections, we proposed an adaptive estimation algorithm of Doppler shifts. A coarse estimation of time invariant coefficients of CIR is given by equation (3.13). However, the existence of estimation errors and synchronization errors is almost inevitable in any estimation algorithm. There still exist synchronization error and estimation inaccuracy which are insolvable by coarse estimation.

In this section, we propose an iterative two-step EM algorithm-based method to solve the joint problem of synchronization parameter estimation and CIR estimation. First, the problem is modeled as a maximum likelihood (ML) problem. Then, an iterative approaching method is used until the result falls within the desired accuracy. Moreover, in this section, we focus on the discussion of a certain Doppler subpath, which can be modeled by a tapped-delay line channel model described in (2.9).

Assume that the estimated synchronization parameter is n_d after initial estimation. Then, the transmitted signal for a certain Doppler subpath can be equivalently expressed as $a(n-n_d)$. The $P-point$ DFT of the transmitted signal is given by

$$S(k) = \sum_{n=0}^{P-1} a(n-n_d) e^{\frac{-j2\pi kn}{P}}. \tag{3.21}$$

Assuming that $m = n - n_d$, the above equation can be rewritten as

$$\begin{aligned} S(k) &= \sum_{m=-n_d}^{P-1-n_d} a(m) e^{\frac{-j2\pi k(m+n_d)}{P}}, \\ &\approx \{\sum_{m=0}^{P-1} a(m) e^{\frac{-j2\pi km}{P}}\} e^{\frac{-j2\pi kn_d}{P}}. \end{aligned} \tag{3.22}$$

We define $\overline{\mathbf{\Omega}}_{n_d} = diag\{\Omega_{n_d}(0), \Omega_{n_d}(1), \ldots, \Omega_{n_d}(P-1)\}$, where $\Omega_{n_d}(k) = e^{\frac{-2\pi jkn_d}{P}}$, and the $P-point$ DFT sequence of original transmitted signal sequence is $\overline{\mathbf{A}} =$

$diag\{A(0), A(1), \ldots, A(P-1)\}$, where $A(k) = \sum_{n=0}^{P-1} a(n) e^{\frac{-j2\pi kn}{P}}$. Then the DFT sequence of equivalent transmitted signal imposed by synchronization error can be expressed as

$$\overline{\mathbf{S}} = \overline{\mathbf{\Omega}}_{n_d} * \overline{\mathbf{A}}. \tag{3.23}$$

If we set

$$n_e = n_d - n_c, \tag{3.24}$$

where n_c is the coarse estimation of synchronization parameter, and n_e denotes the estimation error between each iteration, equation (3.23) can be rewritten as

$$\overline{\mathbf{S}} = \overline{\mathbf{\Omega}}_{n_e} * \overline{\mathbf{F}}, \tag{3.25}$$

where

- $\overline{\mathbf{F}}$ is given by $\overline{\mathbf{\Omega}}_{n_c} * \overline{\mathbf{A}}$,
- $\overline{\mathbf{\Omega}}_{n_c} = diag\{\Omega_{n_c}(0), \Omega_{n_c}(1), \ldots, \Omega_{n_c}(P-1)\}$, $\Omega_{n_c}(k) = e^{\frac{-2\pi jkn_c}{P}}$,
- $\overline{\mathbf{\Omega}}_{n_e} = diag\{\Omega_{n_e}(0), \Omega_{n_e}(1), \ldots, \Omega_{n_e}(P-1)\}$, $\Omega_{n_e}(k) = e^{\frac{-2\pi jkn_e}{P}}$.

During the i^{th} iteration, assuming that the estimated channel impulse response vector is $\overline{\mathbf{h}}^i = \{h_1^i, h_2^i, \ldots, h_L^i\}^T$, we have the channel frequency response (CFR) as

$$\overline{\mathbf{H}}^i = \overline{\mathbf{T}} * \overline{\mathbf{h}}^i, \tag{3.26}$$

where $\overline{\mathbf{T}}$ is the discrete Fourier transform matrix of size $P \times L$ whose element is $T(i,j) = e^{\frac{-2\pi j(i-1)(j-1)}{P}}$. The frequency response of transmitted signal after passing through the estimated channel can be expressed as

$$\overline{\mathbf{R}}_{\mathbf{est}} = \overline{\mathbf{S}} * \overline{\mathbf{H}}^i. \tag{3.27}$$

Hence, the maximum likelihood problem can be converted to a problem in finding a n_d and $\overline{\mathbf{h}}^i$ which can maximize the expectation of the correlation of the estimated received signal $\overline{\mathbf{R}}_{\mathbf{est}}$ and the real received signal $\overline{\mathbf{R}}$. Furthermore, when $\overline{\mathbf{R}}$ and $\overline{\mathbf{R}}_{\mathbf{est}}$ have the maximum correlation, the real part of desired expectation, denoted as $\Re\{\mathbf{E}\left[\overline{\mathbf{R}}^H * \overline{\mathbf{R}}_{\mathbf{est}}\right]\}$, will have the peak value.

$$\begin{aligned}
\Re\{\mathbf{E}\left[\overline{\mathbf{R}}^H * \overline{\mathbf{R}}_{\mathbf{est}}\right]\} &= \Re\{\mathbf{E}\left[\overline{\mathbf{R}}^H * \overline{\mathbf{\Omega}}_{n_e} * \overline{\mathbf{F}} * \overline{\mathbf{H}}^i\right]\}, \\
&\approx \Re\{\frac{1}{P}\sum_{k=0}^{P-1} R^*(k)F(k)H^i(k)e^{\frac{-j2\pi n_e k}{P}}\}, \\
&\approx -(n_e^i)^2\left\{\frac{2\pi^2}{P^3}\sum_{k=0}^{P-1} k^2\Re\left[R^*(k)F(k)H^i(k)\right]\right\} \\
&+ n_e^i\left\{\frac{2\pi}{P^2}\sum_{k=0}^{P-1} k\Im\left[R^*(k)F(k)H^i(k)\right]\right\} \\
&+ \frac{1}{P}\sum_{k=0}^{P-1}\Re\left[R^*(k)F(k)H^i(k)\right]. \qquad (3.28)
\end{aligned}$$

The expression of $\Re\{\mathbf{E}\left[\overline{\mathbf{R}}^H * \overline{\mathbf{R}}_{\mathbf{est}}\right]\}$ is shown in equation (3.28). Maclaurin series expansion $e^{\frac{-j2\pi n_e k}{P}} \approx 1 - j\frac{2\pi n_e}{P}k + \frac{1}{2}\left(j\frac{2\pi n_e}{P}k\right)^2$ is utilized to simplify equation (3.28). The resulting equation can be written in the quadratic polynomial form as

$$\Re\{\mathbf{E}\left[\overline{\mathbf{R}}^H * \overline{\mathbf{R}}_{\mathbf{est}}\right]\} = A(n_e^i)^2 + B(n_e^i) + C, \qquad (3.29)$$

where

$$\begin{aligned}
A &= -\frac{2\pi^2}{P^3}\sum_{k=0}^{P-1} k^2\Re\left[R^*(k)F(k)H^i(k)\right], \\
B &= \frac{2\pi}{P^2}\sum_{k=0}^{P-1} k\Im\left[R^*(k)F(k)H^i(k)\right], \\
C &= \frac{1}{P}\sum_{k=0}^{P-1}\Re\left[R^*(k)F(k)H^i(k)\right].
\end{aligned}$$

Therefore, to obtain the maximum value of equation (3.28), we have

$$n_e^{i+1} = \mathbf{arg}\, max_{n_e}\Re\{\mathbf{E}\left[\overline{\mathbf{R}}^H * \overline{\mathbf{R}}_{\mathbf{est}}\right]\},$$

$$
\begin{aligned}
&= -\frac{B}{2A}, \\
&= \frac{P}{2\pi}\frac{\sum_{k=0}^{P-1} k\Im\left[R^*(k)F(k)H^i(k)\right]}{\sum_{k=0}^{P-1} k^2\Re\left[R^*(k)F(k)H^i(k)\right]}.
\end{aligned} \tag{3.30}
$$

During each iteration, the CIR is updated based on the updated estimation of synchronization parameter. The channel estimation of the i^{th} iteration is expressed as [44]

$$
\overline{\mathbf{h}}^i = \frac{\overline{\mathbf{T}}^H * \overline{\mathbf{F}}^H * \overline{\mathbf{\Omega}}^H_{n_e^i} * \overline{\mathbf{R}}}{\Re\left[\sigma_N^2 \overline{\mathbf{E}}_h^{(-1)} + \left(\overline{\mathbf{F}} * \overline{\mathbf{T}}\right)^H \left(\overline{\mathbf{F}} * \overline{\mathbf{T}}\right)\right]}. \tag{3.31}
$$

In equation (3.31), $\overline{\mathbf{E}}_h = \mathbf{E}\{\overline{\mathbf{h}} * \overline{\mathbf{h}}^H\}$ denotes the power distribution of subpaths. Based on the coarse estimation of CIR depicted using equation 3.13, the estimation of $\overline{\mathbf{E}}_h$ can be calculated for real-time applications.

The joint estimation of the synchronization parameter and CIR can be used as a frequency offset estimation algorithm in OFDM systems with very minor modification [44]. This feature enables a generic frequency domain equalizer when SDR technology is used. The architecture of the design will be discussed in detail in the next section.

3.5 Proposed SDR receiver architecture

Based on the previous analysis, we can merge the processing for two different systems using the similar frequency domain estimation and equalization algorithms. In this section, we investigate a common practical receiver structure for both DC-CDMA/OFDM systems. The proposed structure of the SDR receiver using one-tap multiplier based FDE in DS-CDMA/OFDM context is shown in Fig. 3.1.

This receiver structure can work well in DS-CDMA systems and OFDM systems. In DS-CDMA systems, the proposed receiver operates as a FDE-based Rake-free

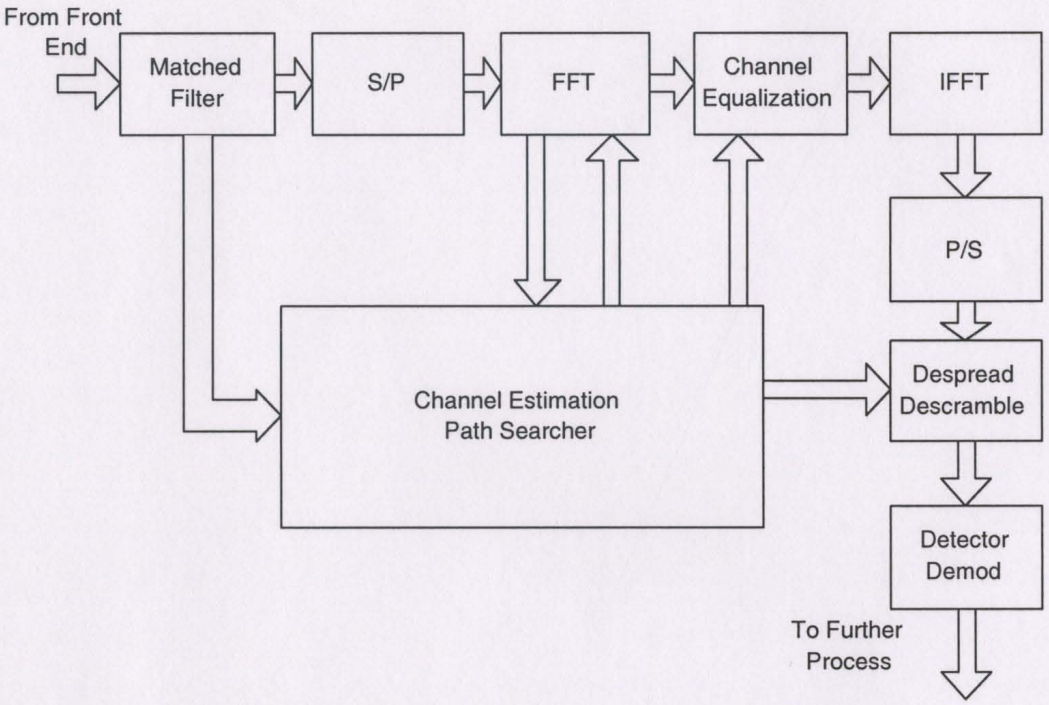

Figure 3.1: The proposed structure of SDR receiver using one-tap multipliers FDE in DS-CDMA/OFDM context

receiver which is able to fully exploit Doppler diversity in frequency domain. In OFDM systems, the proposed receiver operates as a standard FDE-based receiver. The detailed discussion will be given in the following sections.

3.5.1 CDMA Mode

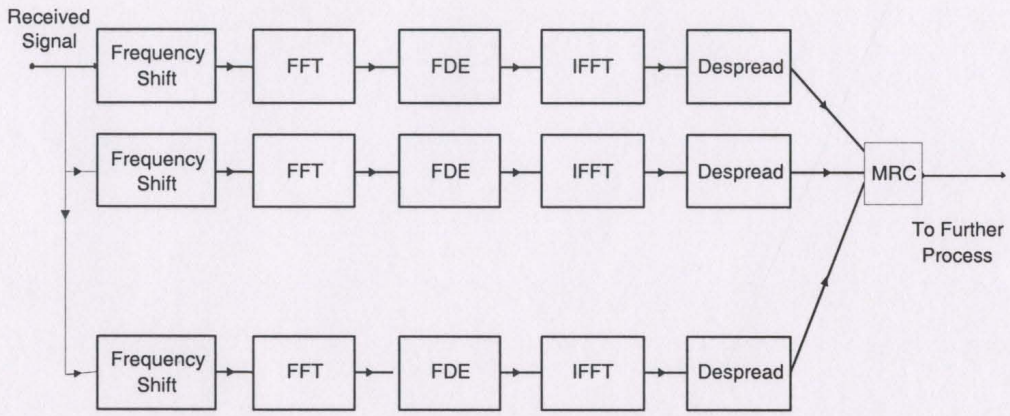

Figure 3.2: The structure of FDE-based receiver architecture

The structure of the FDE-based receiver architecture is shown in Fig.3.2. The amount of frequency shift can be estimated by the proposed adaptive method in Section 3.3. The amount of time shift and distortion can be estimated by the proposed joint estimation of synchronization parameter and CIR algorithm in Section 3.4. Moreover, as proved in [16], the frequency-shifted version of the transmitted signal are orthogonal to each other in DS-CDMA systems. Therefore, the Doppler diversity can be exploited by the maximum ratio combination (MRC) of multiple branches which are dedicated to the receipt of different frequency-shifted copies.

As shown in Fig. 3.2,the number of branches of the proposed receiver structure is based on the number of Doppler subpaths exploited. For each branch, the *Frequency shift* module counters the Doppler effect caused by fast fading channel. For exam-

ple, assuming the first branch is used to receive a copy of transmitted signal whose frequency-shift is $f_e(q)$, the output of the *Frequency shift* module is

$$r'(n) = r(n)\{e^{-\frac{j2\pi n f_e(q)}{P}}\}^*, \tag{3.32}$$

where $r(n)$ is the received signal, and P is the length of DFT. Then, $r'(n)$ will be sent to frequency domain equalizer after passing through FFT module.

Assuming that the final channel estimation of CIR is $\overline{\mathbf{h}}$ and its corresponding $P-point$ DFT sequence is $\overline{\mathbf{H}}$, the Minimum Mean Square Error (MMSE) frequency domain equalization can be expressed as

$$\widehat{R}(k) = \frac{R'(k)H^*(k)e^{\frac{2\pi n_d k}{P}}}{|H(k)|^2 + \sigma_N^2}, \tag{3.33}$$

where $R'(k)$ is the k^{th} signal of $P-point$ DFT sequence of $r'(n)$. Variable n_d is the estimated synchronization parameter. Parameter k denotes the index of discrete frequency, and $\widehat{R}(k)$ denotes the received signal equalized by FDE. Variable σ_N^2 denotes the power of total noise.

When used in DS-CDMA systems, the *Channel Estimation* module receives information from two modules: *Matched Filter* module and *FFT* module. The information from the *Matched Filter* module is used to provide initial channel estimation $\widehat{\mathbf{h}}$. The *FFT* module provides the *Channel Estimation* module with the channel frequency response $\widehat{\mathbf{H}}$ through performing Fourier transform of the estimated discrete CIR.

In return, the *Channel Estimation* module provides the estimated discrete CIR $\widehat{\mathbf{h}}$ to the FFT module to obtain the estimated channel frequency response $\widehat{\mathbf{H}}$. The estimated Doppler shifts and synchronization parameters from the *Channel Estimation* module are also sent to the one-tap multiplier based FDE *Channel Equalization* module.

In this way, the *Channel Equalization* module is able to exploit the Doppler diversity in the frequency domain. The channel equalization parameters are provided

and updated by the *Channel Estimation* module.

Due to a better estimation of synchronization parameter and channel impulse response, the necessity of Rake receiver is eliminated. Consequently, a simple *Despread* module substitutes the costly Rake module in the proposed FDE-based receiver structure.

3.5.2 OFDM Mode

Frequency domain channel estimation and frequency offset estimation in multi-carrier communications system have been extensively studied. Similar to the previous discussion, a joint estimation of frequency offset and CIR via EM algorithm has been proposed in [44]. This algorithm is improved here by providing the initial CFR from equation (3.7) and the initial frequency offset estimation using the redundancy generated by the cyclic prefix [45]. The detailed channel estimation algorithm for OFDM systems is not the concern of this thesis. Therefore, we simply assume that the estimated CFR is $H(k)$ and the estimated frequency shift is f_d. Equation (3.34) is used to mitigate the distortion and frequency shift due to fast fading channels. The equalized signal through FDE, $\widehat{R}(k)$, is given by

$$\widehat{R}(k) = \frac{R(k)H^*(k)e^{\frac{2\pi f_d k}{P}}}{|H(k)|^2 + \sigma_N^2}, \tag{3.34}$$

where $R(k)$ is the k^{th} signal of $P - point$ FFT sequence of received signal $r(n)$. f_d is the estimated frequency offset. k denotes the index of discrete frequency, and σ_N^2 denotes the power of total noise.

When operating in OFDM systems, the *Despread* module and *IFFT* modules are simply bypassed. This is easy to implement using the SDR technology as major receiver modules and computational tasks are defined in software and the communication between them is simply by application programming interface (API) function

calls [3].

More parallelism can be exploited with this architecture because of the introduction of the FFT/IFFT module. Moreover, the reuse of function modules in different systems is another important feature of this architecture. For example, the FFT/IFFT module can be used not only in an OFDM transceiver as modulation/demodulation, but also in a DS-CDMA receiver to facilitate the work of the Channel Equalizer module.

3.6 Summary

In this section, we investigated the generic channel estimation and equalization problem under slow fading channels and fast fading channels in DS-CDMA/OFDM composite radio environments. Firstly, we briefly reviewed some work related with channel estimation and equalization in frequency domain. Then, an investigation was given on the channel estimation and equalization under slow fading channels for both DS-CDMA systems and OFDM systems. Furthermore, by using BEM model, we proposed an EM-based adaptive estimation algorithm for Doppler shifts in DS-CDMA systems. Moreover, an EM-based joint estimation of synchronization parameter and channel impulse response in DS-CDMA sytems is proposed. Based on these algorithms, we developed an innovative generic receiver structure with frequency domain channel equalizer for both DS-CDMA systems and OFDM systems. Not only can this receiver structure provide good performance in OFDM systems, but also it can exploit the inherent Doppler diversity in CDMA systems to further improve the performance while working in DS-CDMA environment.

Chapter 4

Performance Analysis

4.1 Performance Analysis

To demonstrate the efficiency of proposed estimation algorithms and equalization schemes, various simulations have been conducted under the DS-CDMA and OFDM simulation environments.

The following parameters are adopted in the DS-CDMA simulation platform:

- Spreading factor is 32;
- The number of transmitted data symbol per frame is 256;
- The number of pilot symbol is 16;
- The number of frames sent per realization is 4000;
- The chip rate is set as 3.14 Mbps;
- Over sample issue is not considered in this thesis.

The following parameters are used in the OFDM simulation platform:

- The number of sub-carriers is 1024, in which 768 sub-carriers are used for information transmission, and 256 sub-carriers on each side are used as guard interval;
- A total of 64 pilot carriers are evenly inserted among the 768 sub carriers;
- The number of data sent on each sub-carrier during one simulation is 4 bits;
- Chip rate is 32Mbps;
- The duration of each simulation case lasts 2000 iterations. Therefore, a total of $1024 \times 4 \times 2000 = 8192000$ data bits are sent at the chip rate of 32Mbps per simulation experiment.

The multipath wireless channel is implemented based on the modified JAKES model [30]. The modulation scheme is QPSK.

4.1.1 The Minimum Square Error (MSE) Analysis of CIR Estimator

The received signal can be expressed as

$$\overline{\mathbf{R}} = \overline{\Omega}_{n_d} * \overline{\mathbf{A}} * \overline{\mathbf{T}} * \overline{\mathbf{h}} + \overline{\mathbf{N}}_r, \tag{4.1}$$

where $\overline{\mathbf{N}}_r$ denotes the white Gaussian noise matrix with $\mathbf{E}[\overline{\mathbf{N}}_r] = \overline{\mathbf{0}}$ and $\mathbf{E}[\| \overline{\mathbf{N}}_r \|^2] = \overline{\sigma_{\mathbf{N}}^2}$. Therefore, the probability density function (PDF) with respect to $\overline{\mathbf{R}}$ can be expressed as

$$p\left(\overline{\mathbf{R}} \mid \overline{\mathbf{h}}, n_d\right) = \frac{1}{(2\pi\sigma_N^2)^{P/2}} \exp\left(-\frac{1}{2\sigma_N^2} \| \overline{\mathbf{R}} - \overline{\Omega}_{n_d} * \overline{\mathbf{A}} * \overline{\mathbf{T}} * \overline{\mathbf{h}} \|^2\right), \tag{4.2}$$

from which we can directly obtain

$$\ln p\left(\overline{\mathbf{R}} \mid \overline{\mathbf{h}}, n_d\right) = -\frac{P}{2} \ln 2\pi - P \ln \sigma_N - \frac{\| \overline{\mathbf{R}} - \overline{\Omega}_{n_d} * \overline{\mathbf{A}} * \overline{\mathbf{T}} * \overline{\mathbf{h}} \|^2}{2\sigma_N^2}. \tag{4.3}$$

Therefore, the Fisher information matrix $\overline{\mathbf{I}}(\overline{\mathbf{h}})$ for the received signal $\overline{\mathbf{R}}$ can be expressed as

$$\overline{\mathbf{I}}(\overline{\mathbf{h}}) = -\mathbf{E}\left[\frac{\partial^2 \ln p(\overline{\mathbf{R}} \mid \overline{\mathbf{h}}, n_d)}{\partial \overline{\mathbf{h}}^2}\right] = \frac{1}{4\sigma_N^2}\mathbf{E}\left[\overline{\Upsilon}^H * \overline{\Upsilon}\right], \tag{4.4}$$

where $\overline{\Upsilon} = \overline{\Omega}_{n_d} * \overline{\mathbf{A}} * \overline{\mathbf{T}} * \overline{\mathbf{C}_\mathbf{h}}^H$ and $\overline{\mathbf{C}_\mathbf{h}} = diag[1+j, 1+j, ..., 1+j]$ with size of $L \times L$. Let us define the CRLB of the estimation of the channel impulse response $\overline{\mathbf{h}}$ as

$$CRLB(\overline{\mathbf{h}}) = tr\left[\overline{\mathbf{I}}(\overline{\mathbf{h}})^{-1}\right]. \tag{4.5}$$

The definition of CRLB for $\overline{\mathbf{h}}$ indicates that this CRLB depends on the estimation of the synchronization parameter which is expressed as $\overline{\Omega}_{n_d}$. This is due to the nonlinear characteristics of the joint estimation of synchronization parameter and CIR. Therefore, the performance of the CIR estimation can only be evaluated with the knowledge of the synchronization parameter. In addition, the accuracy of the synchronization parameter estimation will affect the local feature of the CIR estimator. The optimization method to improve the estimation accuracy of synchronization parameter will be discussed in details in section 4.1.2.

The MSE performance of the proposed channel estimation is shown in Figure 4.1, where $n_d = 0$. Due to the ML nature of the CIR estimator, the CIR estimation MSE drops close to the CRLB as the SNR increases [46]. Moreover, with the aid of synchronization parameter estimator, the MSE of our CIR estimator converges quickly. When the SNR is beyond 0 dB, the MSE curve almost reaches the CRLB.

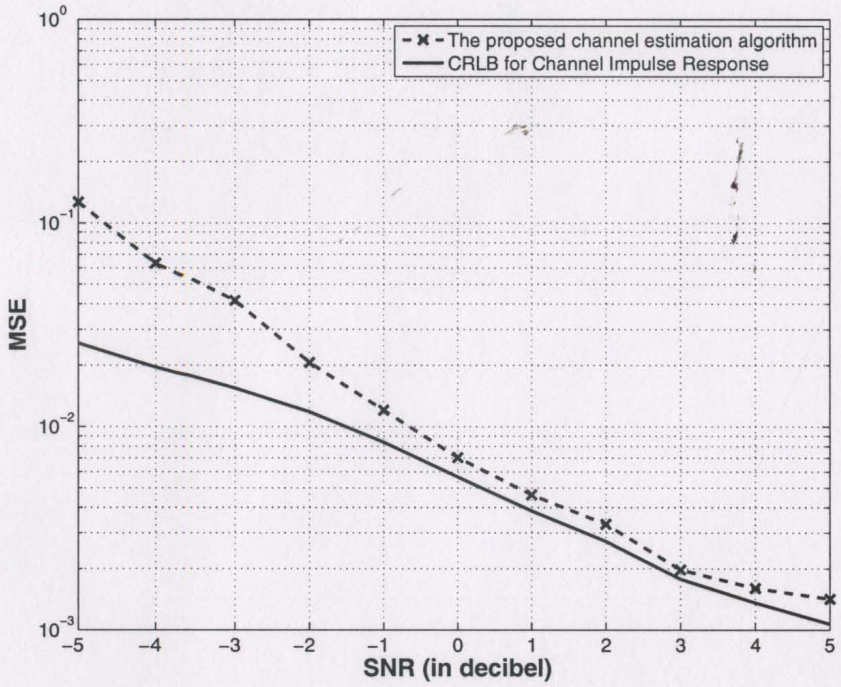

Figure 4.1: The performance of the proposed channel estimation for channel impulse response

4.1.2 The MSE Analysis of Synchronization Parameter Estimator

Let us define

$$\begin{cases} \dfrac{\partial}{\partial n_d}\overline{\mathbf{\Omega}}_{n_d} = \dot{\overline{\mathbf{\Omega}}}_{\mathbf{n_d}} \\ \dfrac{\partial^2}{\partial n_d^2}\overline{\mathbf{\Omega}}_{n_d} = \ddot{\overline{\mathbf{\Omega}}}_{\mathbf{n_d}} \end{cases} \tag{4.6}$$

Therefore, we have

$$\begin{cases} \frac{\partial}{\partial n_d}\overline{\mathbf{\Omega}}^H_{n_d} = \{\dot{\overline{\mathbf{\Omega}}}_{\mathbf{n_d}}\}^H \\ \frac{\partial^2}{\partial n_d^2}\overline{\mathbf{\Omega}}^H_{n_d} = \{\ddot{\overline{\mathbf{\Omega}}}_{\mathbf{n_d}}\}^H \end{cases} \tag{4.7}$$

From equation (4.1), we can obtain the Fisher information matrix $\overline{\mathbf{I}}(n_d)$ for the received signal $\overline{\mathbf{R}}$ as given in equation (4.8).

$$\begin{aligned}
\overline{\mathbf{I}}(n_d) &= -\mathbf{E}[\frac{\partial^2 \ln p(\overline{\mathbf{R}} \mid \overline{\mathbf{h}}, n_d)}{\partial n_d^2}], \\
&= \frac{1}{2\sigma_N^2}\overline{\mathbf{h}}^H * \overline{\mathbf{T}}^H * \overline{\mathbf{A}}^H * [\{\ddot{\overline{\Omega}}_{\mathbf{n_d}}\}^H * \overline{\Omega}_{n_d} + \overline{\Omega}_{n_d}^H * \ddot{\overline{\Omega}}_{\mathbf{n_d}}] * \overline{\mathbf{A}} * \overline{\mathbf{T}} * \overline{\mathbf{h}} \\
&+ \frac{1}{\sigma_N^2}\overline{\mathbf{h}}^H * \overline{\mathbf{T}}^H * \overline{\mathbf{A}}^H * \{\dot{\overline{\Omega}}_{\mathbf{n_d}}\}^H * \dot{\overline{\Omega}}_{\mathbf{n_d}} * \overline{\mathbf{A}} * \overline{\mathbf{T}} * \overline{\mathbf{h}} \\
&- \frac{1}{2\sigma_N^2}\overline{\mathbf{h}}^H * \overline{\mathbf{T}}^H * \overline{\mathbf{A}}^H * \{\ddot{\overline{\Omega}}_{\mathbf{n_d}}\}^H * \mathbf{E}[\overline{\mathbf{R}}] \\
&- \frac{1}{2\sigma_N^2}\mathbf{E}[\overline{\mathbf{R}}^H] * \ddot{\overline{\Omega}}_{\mathbf{n_d}} * \overline{\mathbf{A}} * \overline{\mathbf{T}} * \overline{\mathbf{h}}. \qquad (4.8)
\end{aligned}$$

Therefore, the CRLB of synchronization parameter is given as

$$CRLB(n_d) = \overline{\mathbf{I}}(n_d)^{-1}, \qquad (4.9)$$

which shows that the CRLB of the synchronization parameter estimation relies on the mean value of received pilot signal, $\mathbf{E}[\overline{\mathbf{R}}]$, the estimated CIR, $\overline{\mathbf{h}}$, and the estimated synchronization parameter matrix, $\overline{\Omega}_{n_d}$. Therefore, the CRLB of the synchronization parameter estimation is a random variable. The CRLB can be achieved at high SNR using maximum likelihood (ML) estimators. However, in our research, we chose EM-based estimator instead of computationally complex ML-based estimator. In Figure 4.2, we set the synchronization parameter as $n_d = 0$. The CRLB of MSE for synchronization parameter estimation is 3.5×10^{-6} at SNR = 0 dB, while the MSE for our EM-based estimator can achieve 1×10^{-4} at the same SNR. The proposed EM-Based synchronization parameter estimator features satisfactory performance with also a low cost.

Equation (4.8) indicates that the synchronization parameter estimator can achieve different CRLBs at different estimated values for synchronization parameter. In one simulation scenario, we set the delay of the wireless channel is nine chips. Figure 4.3

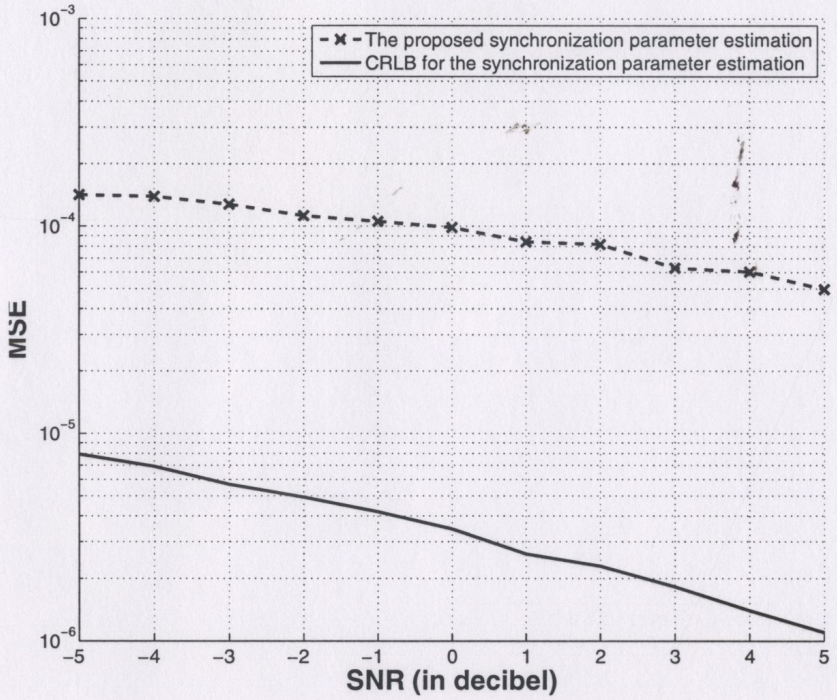

Figure 4.2: The performance of the proposed estimation for synchronization parameter

shows the CRLBs when $n_d = 0$, $n_d = 9$ (for perfect estimation) and n_d is real-time value. It shows that the CRLB of perfect estimation is the lowest. Also, it reveals that, by choosing different initial synchronization parameters, the performance of the synchronization parameter estimator can be improved. For example, using the same estimation algorithm, the CRLB for $n_c = n_d = 9$ is much lower than the CRLB for $n_c = n_d = 0$.

Figure 4.4, which proves our conjecture, shows the MSE of the synchronization parameter estimator at SNR = 5 dB over the initial estimation range $n_c \in [0, 34]$. n_c is measured in terms of chip duration ($\frac{1}{3.14} \times 10^{-6}$ second). The CRLB for the synchro-

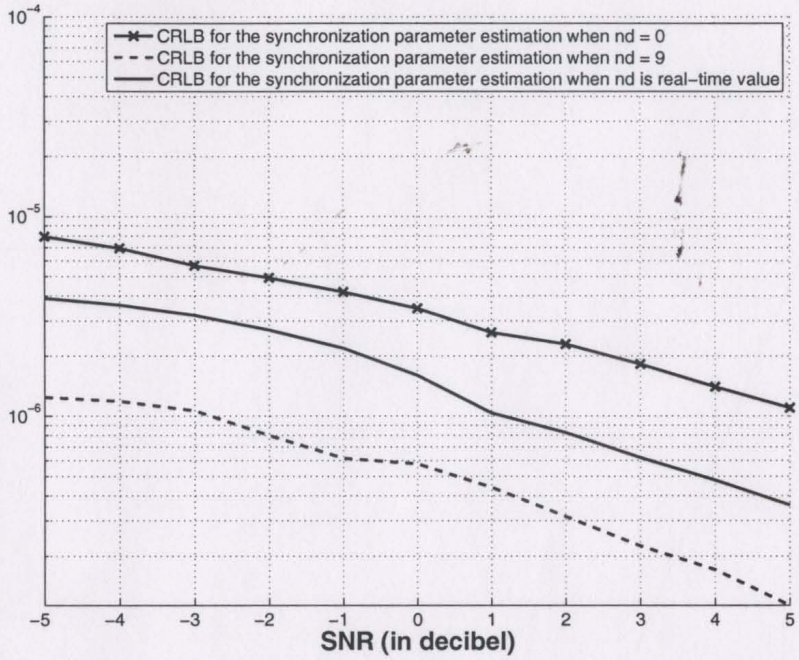

Figure 4.3: The CRLB at different synchronization parameters

nization parameter estimation is given by the mean value over the range $n_c \in [0, 34]$, which is 3.2×10^{-7}. Figure 4.4 shows that the MSE of estimator changes tremendously as n_c varies. When $n_c = 6$, the MSE of the estimator achieves its minimum value 6.1×10^{-7}. Therefore, in this scenario, $n_c = 6$ is the optimum configuration of the synchronization parameter estimator. It is noted that the optimum value of n_c varies under different communication scenarios. This value can be coarsely obtained by the path searcher module in DS-CDMA receivers.

4.1.3 The Illustration of the Shift-and-correlation Procedure

In slow fading channels, channel estimation in DS-CDMA systems is based on a shift-and-correlation procedure. The same procedure is also required in the traditional

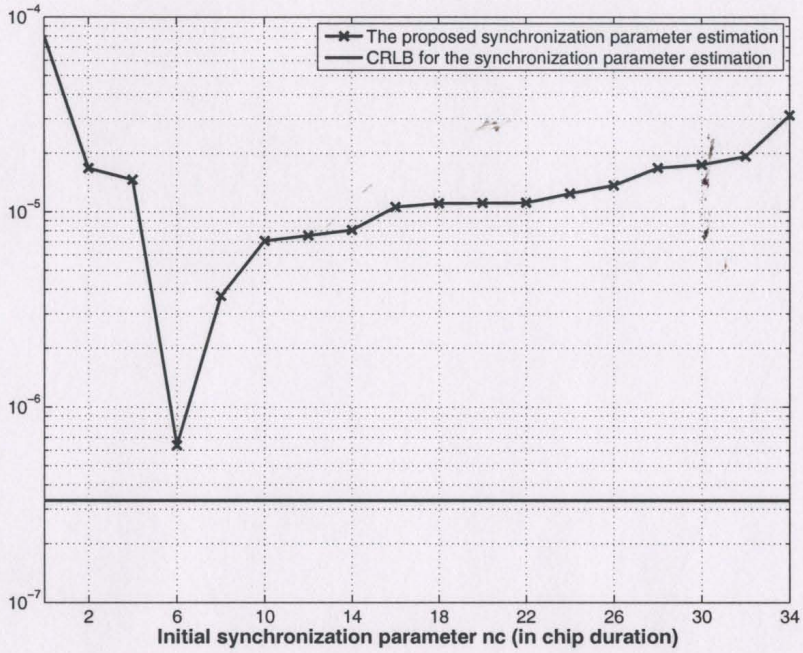

Figure 4.4: MSE versus different initial synchronization parameter values at SNR = 5 dB

Rake-based receiver to provide the time-shift information for Rake fingers. The output $\mathbf{E}\{y(m)\}$ of a typical shift-and-correlation procedure is shown in Fig. 4.5. The mathematical form of $\mathbf{E}\{y(m)\}$ is given by

$$\begin{aligned} \mathbf{E}\{y(m)\} &= \mathbf{E}\{\frac{1}{W}\sum_{n=1}^{W}\sum_{l=1}^{L} h_l \delta(m - \left[\frac{\tau_l}{T_c}\right])\} + \mathbf{E}\{N_r\}, \\ &\approx \frac{1}{W}\sum_{n=1}^{W}\sum_{l=1}^{L} h_l \delta(m - \left[\frac{\tau_l}{T_c}\right]). \end{aligned} \tag{4.10}$$

In Fig. 4.5, the width of correlation, W, is set as $320 \times T_c$, where T_c is the chip period. Parameter m denotes the length of shift, which is also the scope of the search. In our study, we set $m \in [0\ 300T_c]$. From equation (4.10), $y(m)$ will achieve peak values when $m = \frac{\tau_i}{T_c}$ and τ_i denotes the delay of the i^{th} subpath, where $i = 1, 2, \ldots, L_c$.

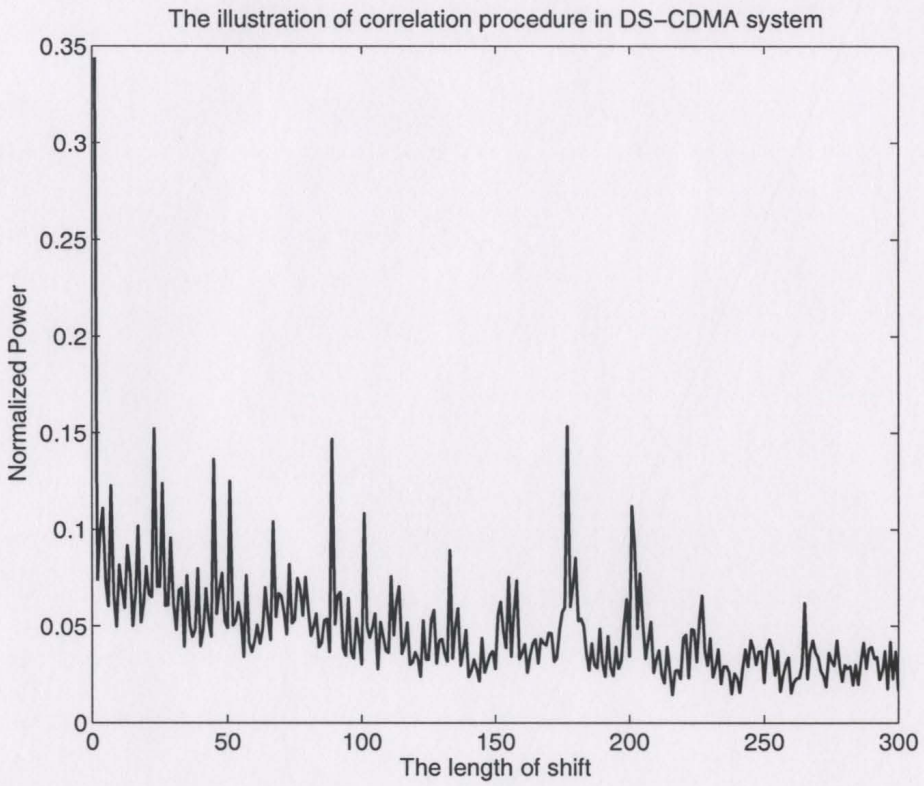

Figure 4.5: The illustration of the shift-and-correlation procedure

This theoretical result is clearly verified by the simulation results shown in Fig. 4.5.

As shown in in the figure, there clearly exist several peak values as the length of shift increases. Moreover, as the length of shift increases, the peak value tends to decrease, although there is some exceptions observed due to some unpredictable noise caused by radio channels. In Fig. 4.5, the most significant four peak values appear at $m = T_c$, $m = 185T_c$, $m = 25T_c$, and $m = 91T_c$, according to the magnitude of signal power. From the distribution of the normalized power of the output, the power distribution function of wireless channels can be well estimated. As shown in the figure, the distribution of the normalized power from a typical shift-and-correlation procedure approximately follows an exponential distribution, the power distribution pattern of the wireless channel in our simulation shown in Fig. 4.6.

4.1.4 The Illustration of the Proposed Estimation Algorithms

An important aspect of the proposed adaptive estimation of Doppler shifts in section 3.3 is that, through manually shifting the columns of the estimated TI coefficient matrix $\overline{\mathbf{H}}_{BEM}$, different f_e (f_{e1}, f_{e2}, and f_{e3} in the case of $Q = 1$), which maximize the corresponding $\mathbf{E}[R^*(k)\tilde{R}(k)]$, can be found by exhaustive searching within a given range. Then, based on the searched values of f_{e1}, f_{e2}, and f_{e3}, the following three independent linear equations can be constructed

$$\begin{aligned}
-\frac{B_1}{2A}f_e(-1) - \frac{B_2}{2A}f_e(0) - \frac{B_3}{2A}f_e(1) - \frac{B_4}{2A} &= f_{e1}, \\
-\frac{B_2}{2A}f_e(-1) - \frac{B_3}{2A}f_e(0) - \frac{B_1}{2A}f_e(1) - \frac{B_4}{2A} &= f_{e2}, \\
-\frac{B_3}{2A}f_e(-1) - \frac{B_2}{2A}f_e(0) - \frac{B_1}{2A}f_e(1) - \frac{B_4}{2A} &= f_{e3},
\end{aligned}$$

where B_1, B_2, B_3, B_4 and A are constants whose definitions can be found in Section 3.3. Fig. 4.7 shows the normalized values of $\mathbf{E}[R^*(k)\tilde{R}(k)]$. In the figure, the solid

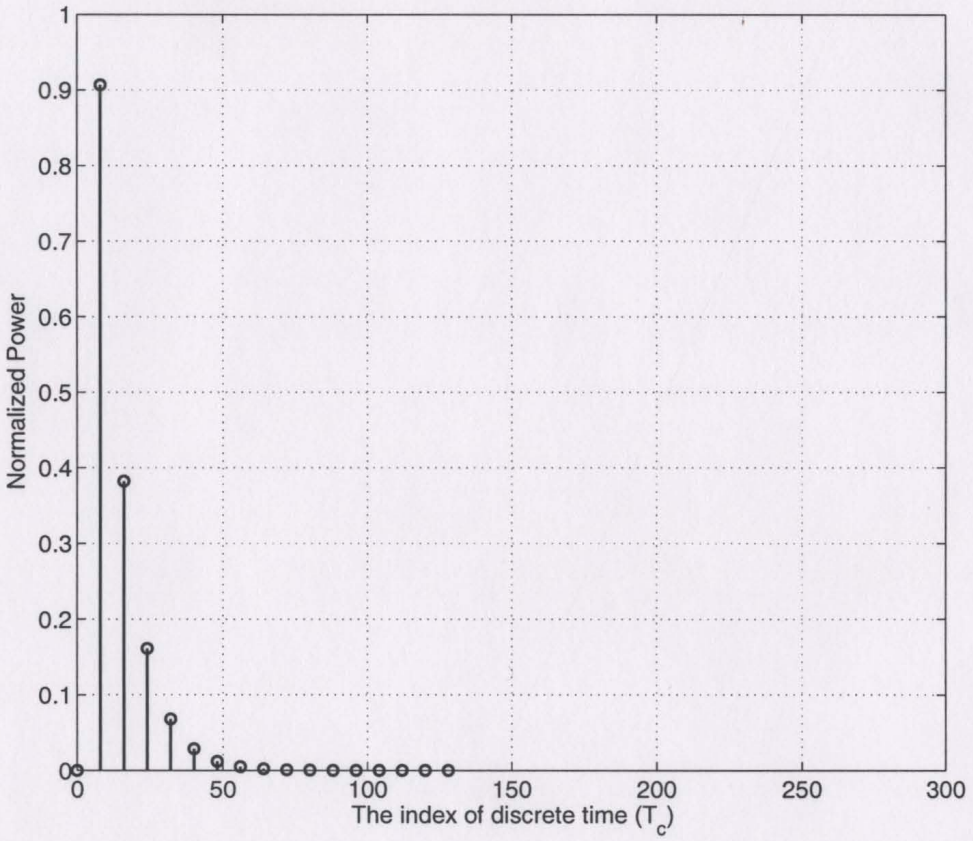

Figure 4.6: The power distribution function of the wireless channel in the simulation

line shows the normalized values of $\mathbf{E}[R^*(k)\tilde{R}(k)]$ based on the original $\overline{\overline{\mathbf{H}}}_{BEM}$. The slashed dot line shows the normalized values of $\mathbf{E}[R^*(k)\tilde{R}(k)]$ based on the $\overline{\overline{\mathbf{H}}}_{BEM}$ circularly shifted to the left by one column, and the slashed line shows the normalized values of $\mathbf{E}[R^*(k)\tilde{R}(k)]$ based on the $\overline{\overline{\mathbf{H}}}_{BEM}$ circularly shifted to the left by two columns. As indicated in Fig. 4.7, $\mathbf{E}[R^*(k)\tilde{R}(k)]$ will have a peak within a given range of f_e. Moreover, as shown in the figure, there exist three distinctive f_e enabling $\mathbf{E}[R^*(k)\tilde{R}(k)]$ to obtain maximum value. Therefore, it is feasible to obtain the corresponding frequency shifts by exhaustive search. Based on the search results, three independent linear equations can be constructed. To illustrate the convergence characteristic of the joint estimation of synchronization parameter and CIR, we provide the convergence curve of mean square error of the estimation in Fig. 4.8. The initial estimation of the synchronization parameter, n_c, and the initial estimation error, n_e, are set to zero. As shown in Fig. 4.8, the mean square error of the estimation converges quickly. For example, the estimation error drops to about 3.5×10^{-3} under 10dB SNR condition. In Section 3.4, we also proposed an iterative method to update the estimation of channel impulse response. The expression of the iterative update is given as

$$\overline{\mathbf{h}}^i = \frac{\overline{\mathbf{T}}^H * \overline{\mathbf{F}}^H * \overline{\mathbf{\Omega}}_{n_e^i}^H * \overline{\mathbf{R}}}{\Re\left[\sigma_N^2 \overline{\mathbf{E}}_h^{(-1)} + \left(\overline{\mathbf{F}} * \overline{\mathbf{T}}\right)^H \left(\overline{\mathbf{F}} * \overline{\mathbf{T}}\right)\right]}. \tag{4.11}$$

According to this expression, the estimated CIR will provide better approximation of the practical CIR as the number of iterations increases. The illustration of the proposed iterative estimation of synchronization parameters and CIR in DS-CDMA systems is shown in Fig. 4.9 and Fig. 4.10. It is shown that the most significant three subpaths ($T = 9T_c$, $T = 17T_c$ and $T = 25T_c$) can be detected in all three scenarios, where the number of iterations is 2, 16, and 32. As indicated by Fig. 4.9 and Fig. 4.10, as the number of iterations increase, the estimation noise decreases.

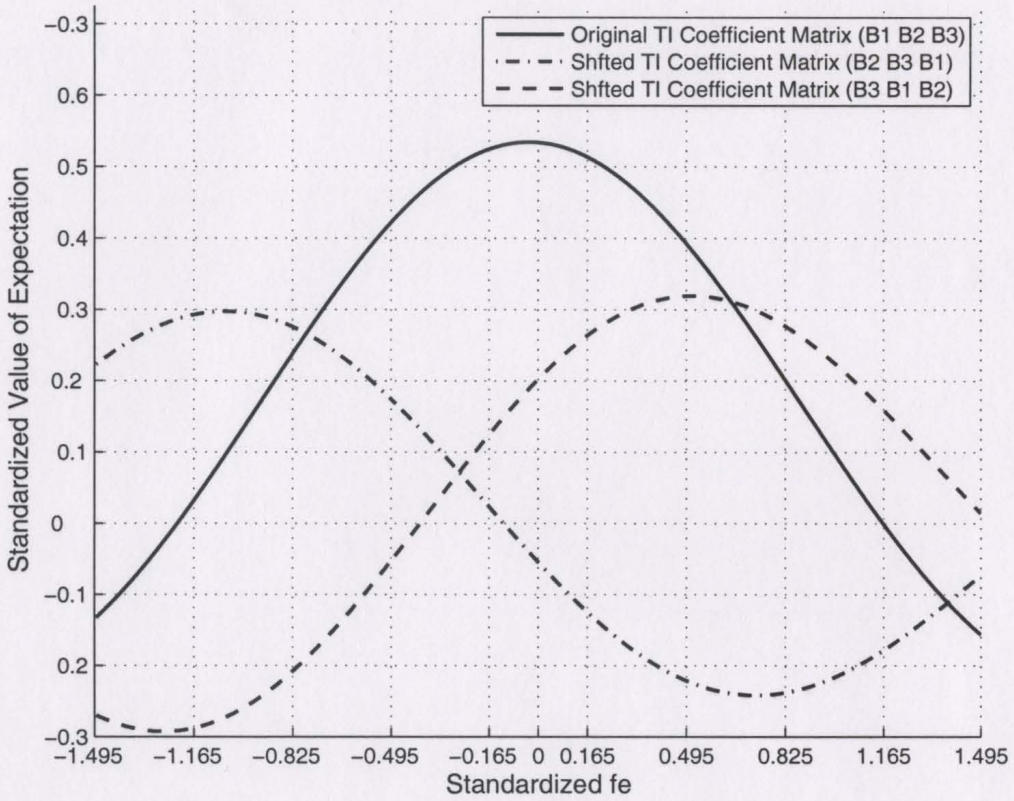

Figure 4.7: The illustration of the proposed adaptive estimation of Doppler shifts

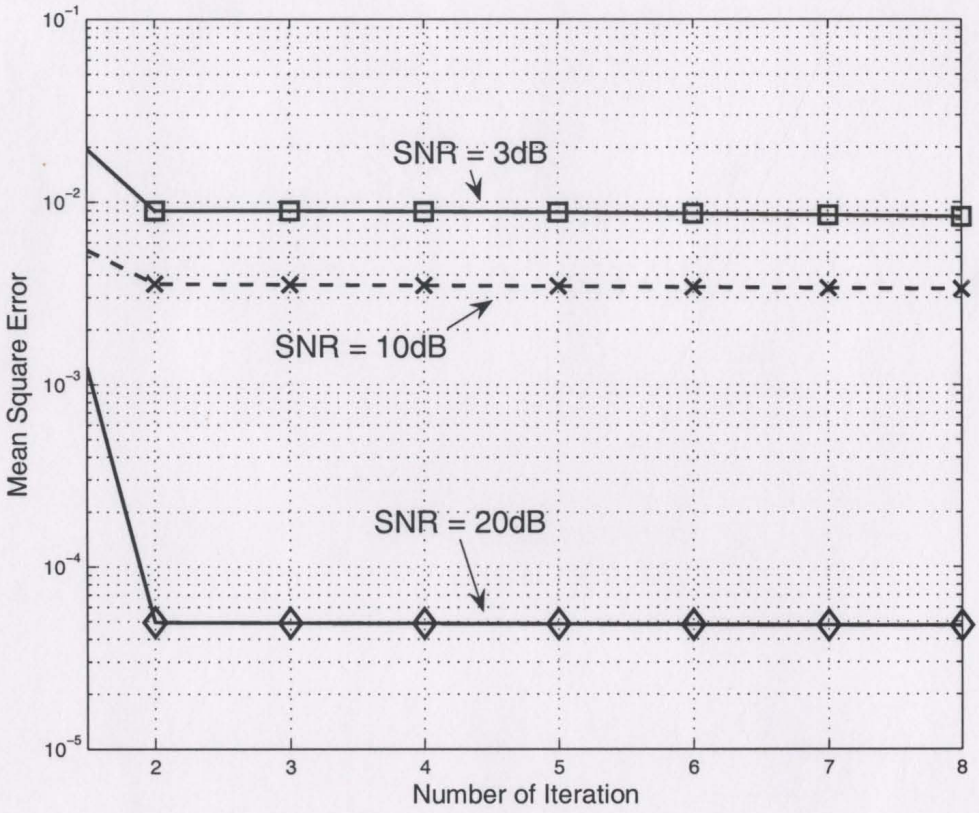

Figure 4.8: The normalized Mean Square Error convergence curve

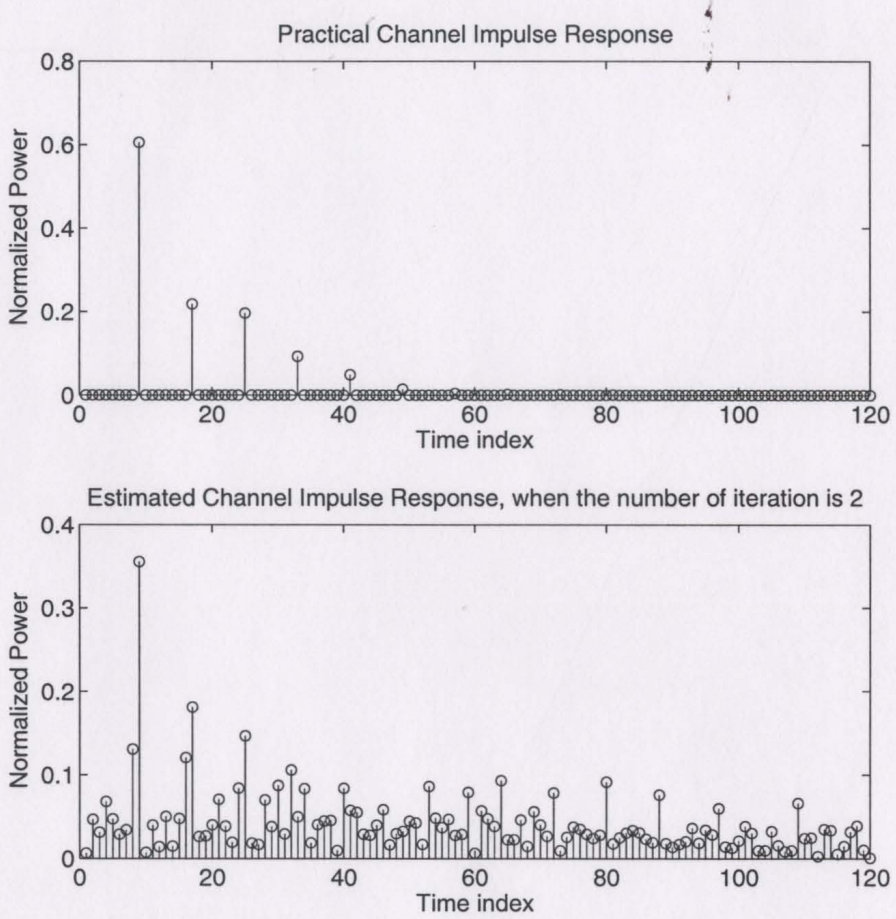

Figure 4.9: The illustration of the proposed iterative estimation of CIR in DS-CDMA systems, when the number of iterations is 2

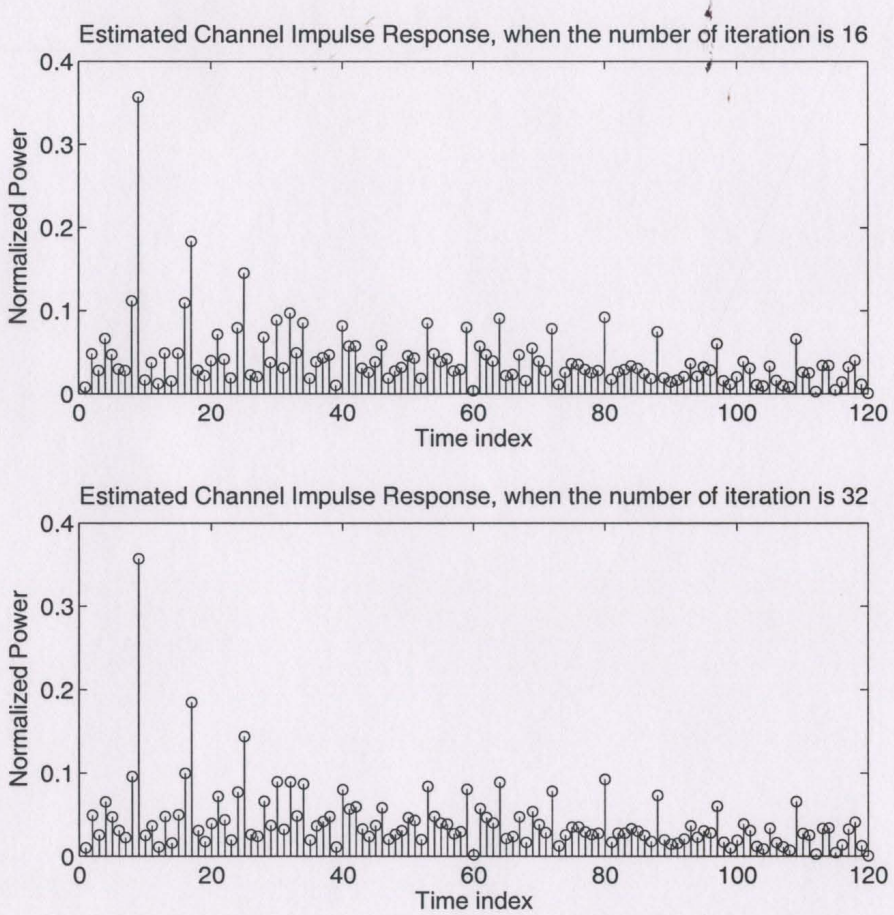

Figure 4.10: The illustration of the proposed iterative estimation of CIR in DS-CDMA systems, when the number of iterations is 16 and 32

For example, using the estimation scheme, there exists a subpath when $T = 8T_c$ in all three scenarios. In fact, it does not exist in practical channel impulse response. Therefore,it is actually part of the estimation noise. In Fig. 4.9, with 2 iterations, the normalized power of this estimation noise is about 0.13. In Fig. 4.10, the normalized power of this estimation noise is reduced to about 0.11 and 0.1 with 16 and 32 iterations, respectively. Other significant estimation noise also follows the similar trend: with more iterations, the estimation noise decreases. Note that one of the main purpose of the proposed iterative estimation is to estimate the synchronization parameter n_d, which is imposed by the radio channels in the form of $e^{\frac{-j2\pi n_d}{P}}$ with power $|e^{\frac{-j2\pi n_d}{P}}|^2 = 1$. Therefore, the estimated distribution of normalized power of channel impulse response will not change significantly with the increase of number of iterations.

4.1.5 Performance Analysis of the Proposed Receiver Structure

Joint Estimation of Synchronization Parameter and CIR (Without Exploiting Doppler Diversity)

To illustrate the efficiency of the proposed channel estimation and equalization scheme, the stellular diagram of received signal after equalization under different SNR values is shown in Fig. 4.11. The velocity of the mobile station is 0, and the number of subpaths is 16. From the figure, we can observe that the stellular blocks of the received signal after equalization converge well when the SNR is as low as 8dB. Therefore, decent performance can be achieved using our proposed estimation and equalization scheme. When SNR increases to 20dB, although the stellular blocks of the received signal after equalization are further converged, the improvement is not very signifi-

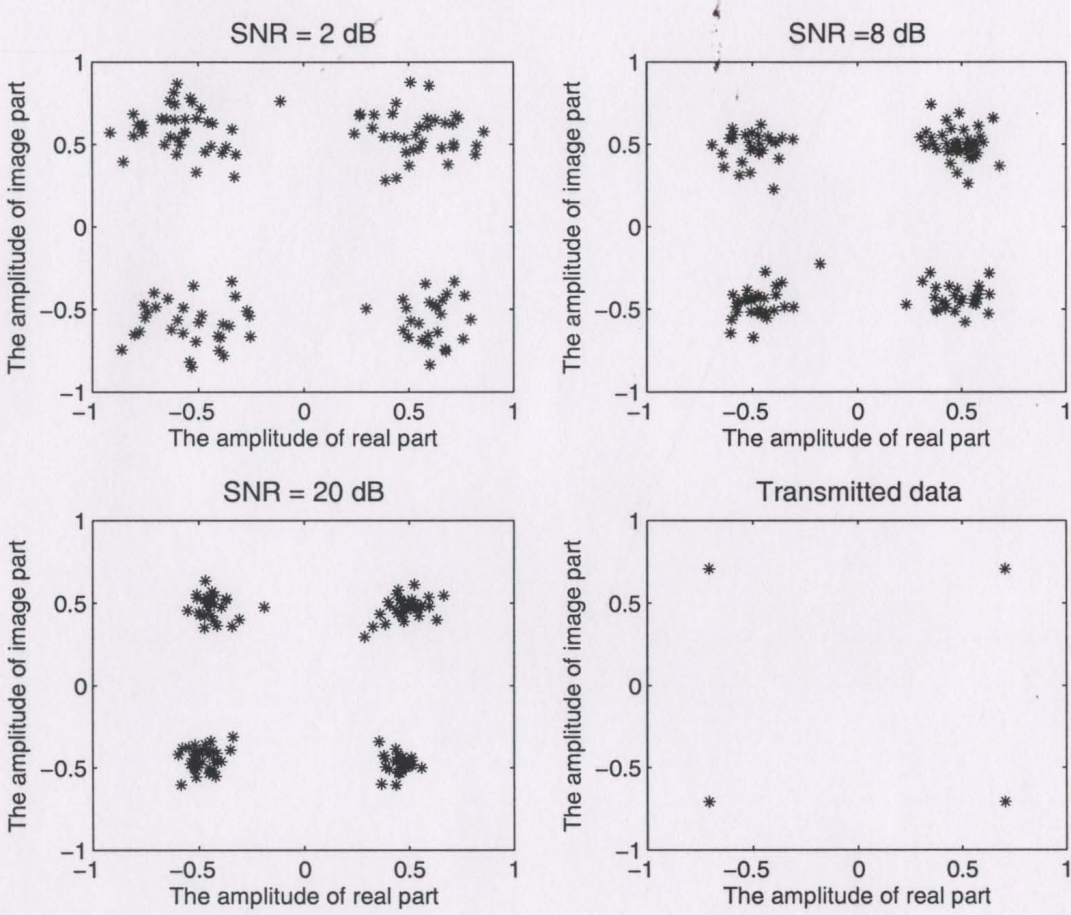

Figure 4.11: The stellular diagram of received signal after equalized at different SNR values

cant. This observation indicates that there exists a threshold of performance as SNR increases. The BER performance curve shown in Fig. 4.12 confirms our conjecture. Due to the fast and precise estimation of the synchronization parameter and CIR,

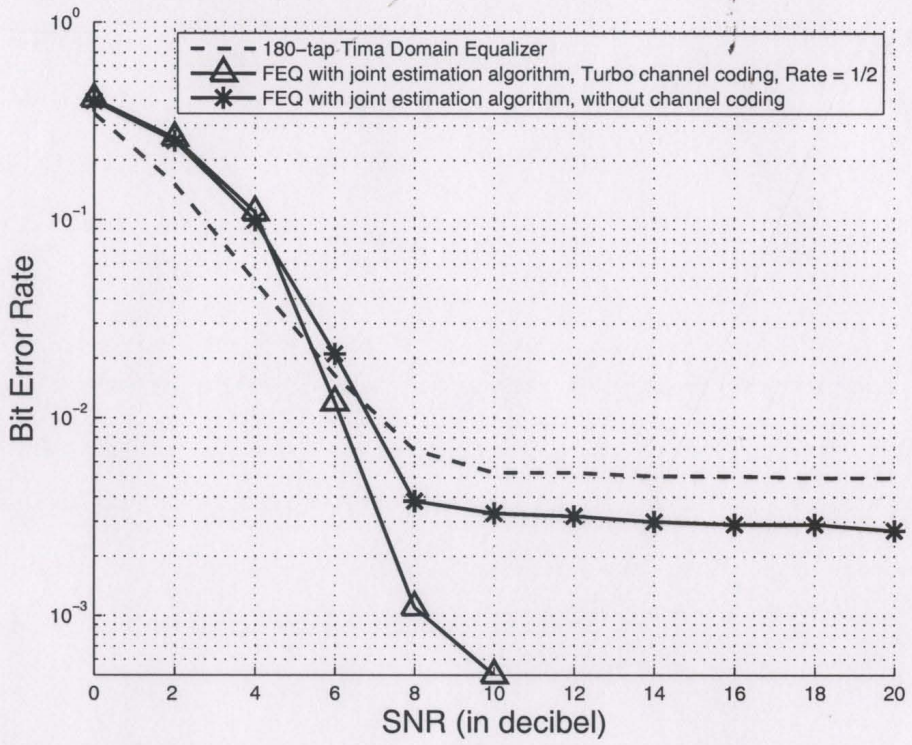

Figure 4.12: The illustration of the enhancement introduced by the proposed joint estimation and FDE in fast fading radio channel

our proposed FDE approach demonstrates superior capability against doubly selectivity of wireless channels when compared with traditional equalization methods. In Fig. 4.12, we plot the BER performance of the proposed algorithm in fast fading channels. It is assumed that the velocity of the mobile station is 40 km/hr. The number of subpaths is 8. In the figure, results from the proposed FDE scheme with and without Turbo channel coding (coding rate = 1/2) and a 180-tap time-domain

equalizer (TDE) are compared. The TDE is based on the MMSE criterion, which can be expressed as follows

$$\mathbf{r}_{TDE-MMSE} = (\overline{\mathbf{h}}^H \overline{\mathbf{h}} + \frac{1}{\sigma_n^2}\overline{\mathbf{I}})^{-1} \overline{\mathbf{h}}^H \overline{\mathbf{r}}, \tag{4.12}$$

where $\overline{\mathbf{h}}$ denotes the estimated channel impulse response, σ_n^2 denotes the power of AWGN, and $\overline{\mathbf{I}}$ denotes an identity matrix. Variable $\overline{\mathbf{r}}$ is the received signal and $\mathbf{r}_{TDE-MMSE}$ is the output of the MMSE-based TDE.

From Fig. 4.12, the performance of receiver using the frequency domain joint estimation algorithm is better than that of a receiver purely using TDE. As indicated in the Fig. 4.12, the threshold of the proposed FDE using joint estimation, which is about 3×10^{-3} when 8 dB, is lower than that of the traditional TDE, which is about 5×10^{-3}. The figure also demonstrates that, because of the relatively more accurate estimation and equalization of the multipath fading effect, the performance of the receiver can be tremendously improved by adopting proper channel coding schemes. For example, with the help of basic Turbo coding scheme, the proposed FDE can obtain a BER better than 1×10^{-3} when SNR $\geq$ 8 dB.

As the velocity of mobile station increases, the estimation accuracy decreases due to many reasons, in particular, the Doppler effect. As shown in Fig. 4.13, assuming the multipath channel is consisted of 6 subpaths, BER saturates at 9×10^{-4}, 8×10^{-3}, and 1×10^{-2} for the speed of 40 km/hr, 80 km/hr, and 120 km/hr, respectively. By using proper channel coding schemes and diversity techniques, the performance of radio receiver in fast fading channel can be further improved. The tremendous improvement introduced by diversity techniques will be presented in the next subsection. In any case, the traditional Rake receiver will be less efficient than both FDE-based and TDE-based receiver architecture [38]. Therefore, we do not demonstrate the performance of the traditional Rake receiver.

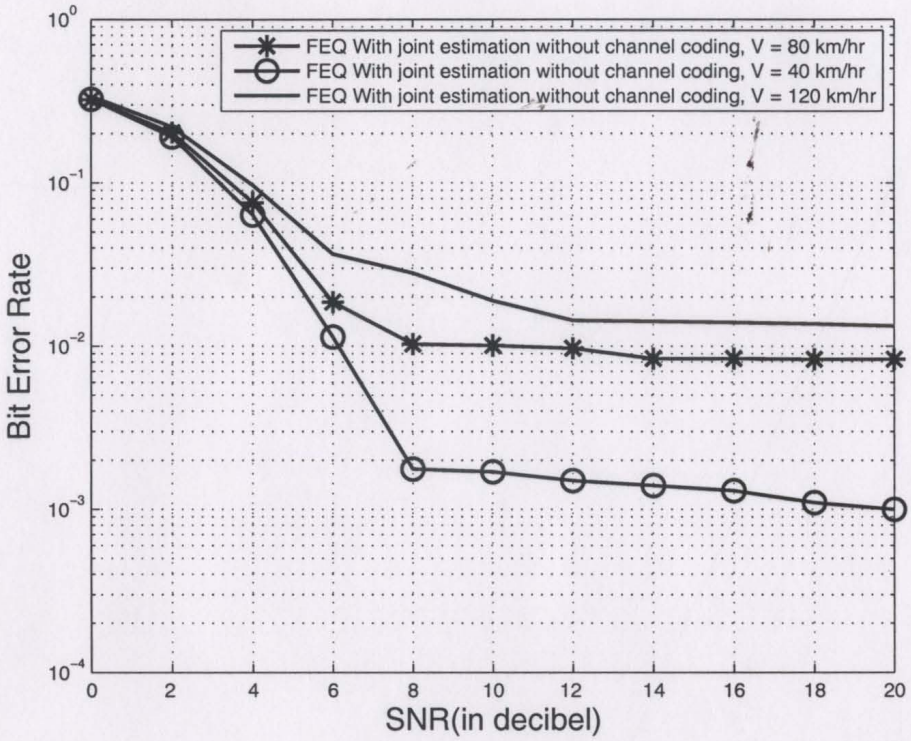

Figure 4.13: The illustration of the influence of mobile velocity on the BER performance

Considering the typical application environment of each system, OFDM technology is often used in the wireless local area network (WLAN) where high data rate, severe frequency selectivity effect, and slow fading radio channel are often expected. While CDMA technology is commonly used in the wide area network (WAN), where moderate data rate, moderate frequency selectivity effect, but fast fading radio channel are often encountered. Therefore, in Fig. 4.14, we plot the BER performance of the comb-type inserted pilot-carriers based FD channel estimation in slow fading channel (32 subpaths) and the proposed FDE with EM algorithm-based adaptive joint estimation in fast fading channels (4 subpaths). From the figure, we observe

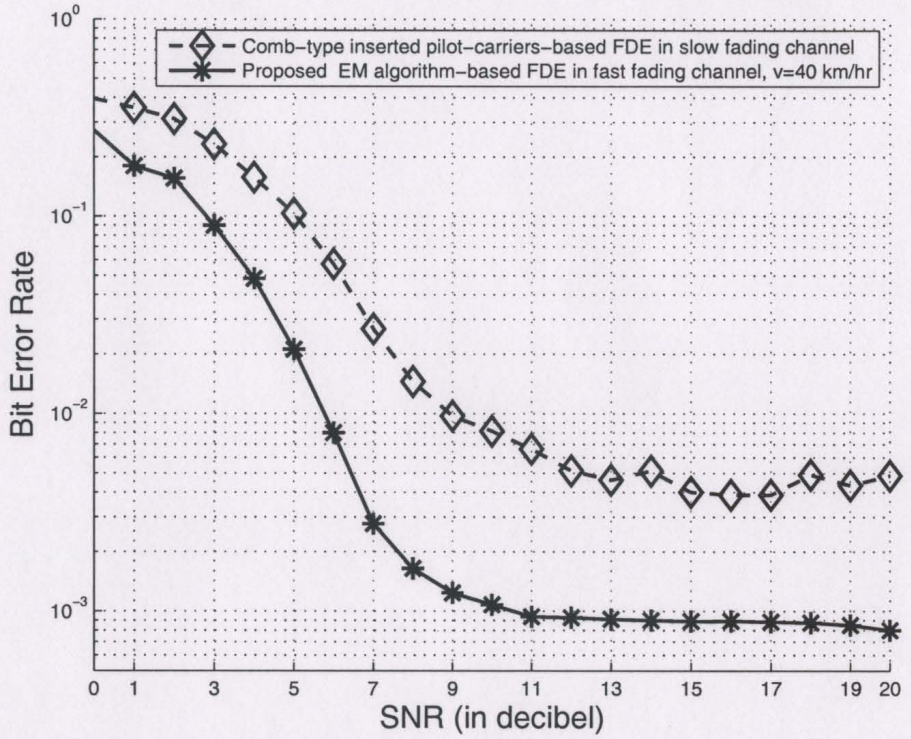

Figure 4.14: The BER performance of proposed FDE scheme in OFDM and CDMA context

that the BER performance of the receiver saturates at 7×10^{-3} and 9×10^{-4} at $11dB$ SNR, when operates in OFDM mode and CDMA mode, respectively. In general, the proposed FDE structure with joint estimation algorithm can achieve desired performance in both CDMA and OFDM systems under slow fading and fast fading channel conditions. Moreover, the performance of the proposed FDE-based receiver can be further improved by exploiting Doppler diversity in frequency domain in the DS-CDMA context.

Joint Estimation of Synchronization Parameter and CIR (With Exploiting Doppler Diversity)

The structure of the frequency domain equalizer to exploit Doppler diversity in DS-CDMA systems is shown in Fig. 3.2. We first compare the stellular diagram of the received equalized signal using different equalization schemes. The stellular diagrams are obtained when SNR = 20 dB, the velocity of the mobile station is 40 km/hr, and the number of subpaths is 16. As shown in Fig. 4.15, the stellular diagram of the received signal equalized by the traditional TDE using 180-tap is obviously rotated because of the Doppler shifts caused by the fast fading channel. Moreover, the amplitude of the received signal is also significantly reduced. Therefore, neither the phase rotation nor the power attenuation caused by the doubly selective channels can be well compensated by the traditional TDE.

On the other hand, as shown in Fig. 4.15, the phase of the received signal equalized by the proposed FDE with joint estimation can be better maintained. Also, the signal attenuation is well compensated. Moreover, with the help of the exploitation of Doppler diversity, the proposed estimation method can even better maintain the phase of the received signal. As shown in the figure, the stellular blocks of the received signal are more concentrated. Therefore, the BER performance of the proposed FDE-

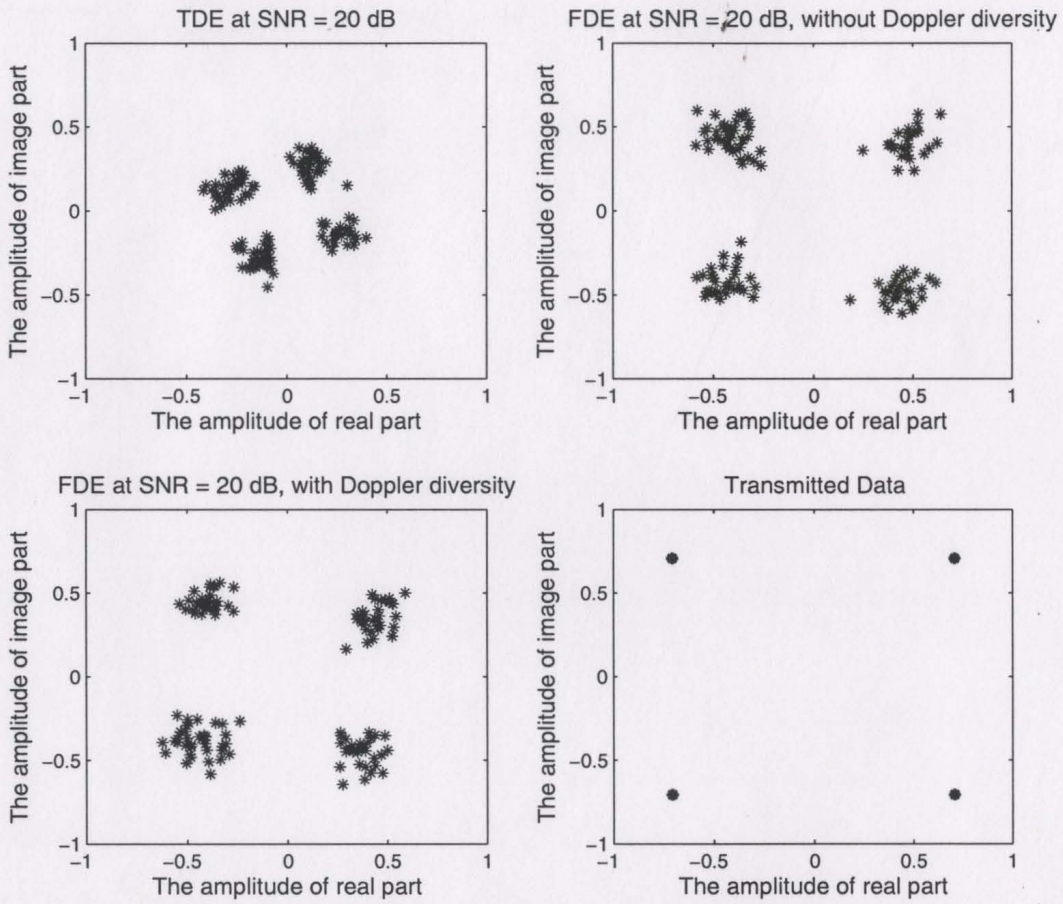

Figure 4.15: The stellular diagram of received signal after equalized

based receiver can be further improved by properly exploiting Doppler diversity. It is necessary to investigate the influence of the velocity of the mobile station on the BER performance of the proposed FDE with joint estimation when exploiting Doppler diversity. Fig. 4.16 gives the stellular diagram of the received signal equalized by the proposed estimation scheme at different velocities. In the BEM model used to describe the doubly selective channel, a total number of 3 Doppler subpaths ($Q = 1$) is considered. In Fig. 4.16, we compare four scenarios where $v = 0$km/hr, $v = 40$km/hr, $v = 80$km/hr, and $v = 120$km/hr, respectively. As the velocity of the mobile station increases, the phase of the received signal is more severely rotated. Because of the high efficiency of the proposed adaptive estimation scheme, the phase rotation is still not significant at a velocity of 40km/hr. However, due to the increasing inaccuracy of the BEM model with $Q = 1$ as the Doppler effects become more severe, the Doppler shifts can not be well compensated when $v = 80$ km/hr and $v = 120$ km/hr. By properly selecting the parameters of the BEM model, such as increasing Q when the velocity of the mobile station increases, the performance of the proposed FDE-based receiver can be further improved under fast fading channels.

The BER performance of the proposed FDE-based receiver structure is given in Fig. 4.17 and Fig. 4.18. In Fig. 4.17, we consider a total number of 16 subpaths and a speed of $40km/hr$. This wireless channel is a typical fast fading channel with severe frequency selectivity and time selectivity. To provide comparison with the traditional receiver structure, the performance of a MMSE-based 180-tap time domain equalizer is also included in the same figure. The traditional TDE is obviously outperformed by the proposed FDE structure under doubly selective channel conditions. For example, with the aid of joint estimation of synchronization parameter and CIR, the proposed FDE without exploiting Doppler diversity could obtain a BER of 3×10^{-3} when $SNR = 8dB$, while traditional TDE can only provide a BER of 7×10^{-3} under

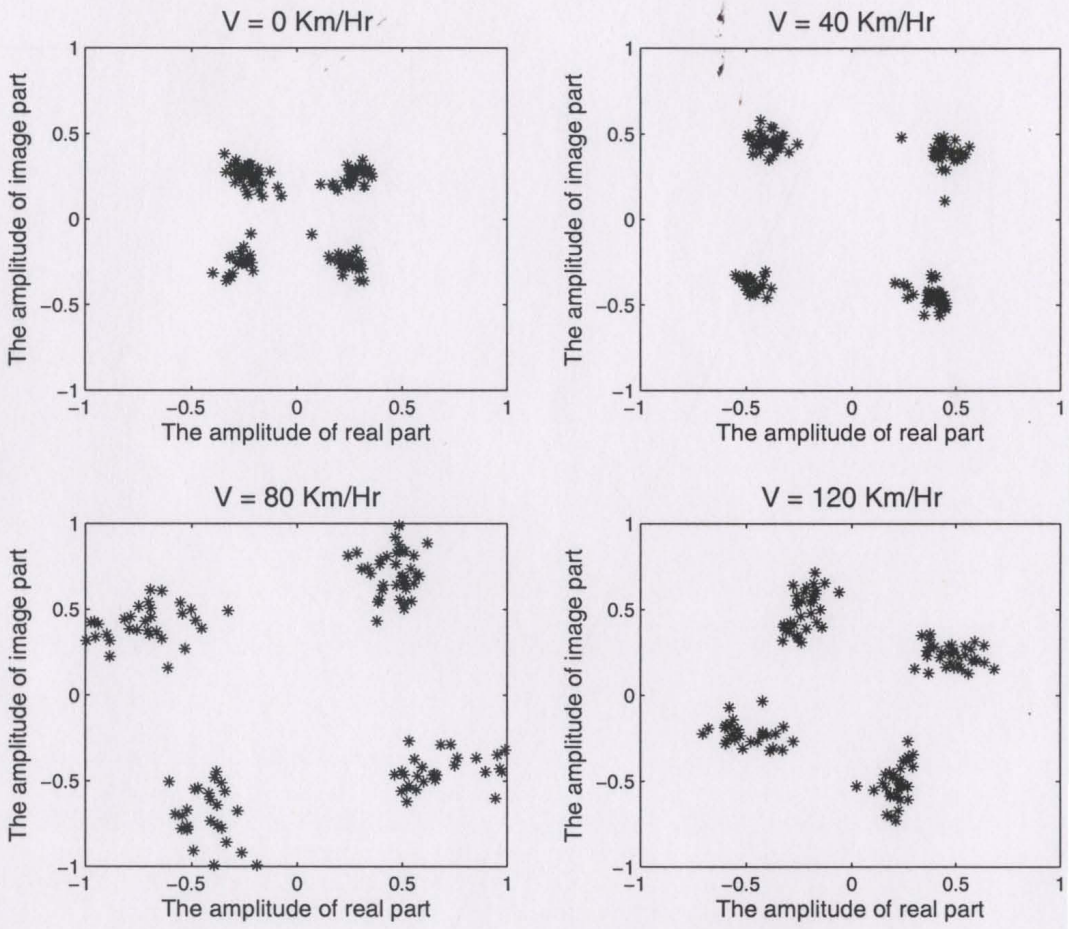

Figure 4.16: The stellular diagram of the received signal after equalized by the proposed FDE with joint estimation when exploiting Doppler diversity

the same condition. Furthermore, if Doppler diversity is added to propose FDE, a tremendous improvement of performance can be achieved. For example, when using the deterministic method of estimating Doppler shifts as described in [31], the proposed FDE exploiting Doppler diversity can obtain a BER of 1×10^{-3} when $SNR = 8dB$. Furthermore, when the proposed adaptive estimation of Doppler shifts is used, the proposed FDE can obtain an outstanding BER of 6×10^{-4} under the same condition. It should be noticed that this impressive performance of the proposed FDE-based receiver is obtained without using over sampling, pulse-shaping filter and channel coding. Thus, the proposed architecture has great potential to achieve better performance when used in a practical composite radio receiver.

To further illustrate the performance of the FDE-based receiver, Fig. 4.18 gives the BER performance of different equalization schemes when the number of subpaths is 16 and the velocity of mobile station is 80 km/hr. Obviously, the proposed FDE-based receiver exploiting Doppler diversity outperforms other equalization schemes. For example, when $SNR = 8dB$, the proposed FDE exploiting Doppler diversity can achieve a BER of 7×10^{-3}, while the FDE based on deterministic estimation of Doppler shifts, FDE without exploiting Doppler diversity, and 180-tap TDE can obtain BER of 9×10^{-3}, 1×10^{-2} and 2.3×10^{-2} under the same condition, respectively.

As shown in Fig. 4.17 and Fig. 4.18, it is noticeable that the TDE outperforms the proposed FDE scheme in low SNR scenario (SNR $\in [0dB, 3dB]$). The reason is that the inherent interpolation error and estimation error of frequency domain equalization is more severe than that of time domain equalization with excessive length. As the SNR increases. the estimation of synchronization parameter, CIR and Doppler shifts in frequency domain becomes more accurate, the proposed FDE scheme ultimately outperforms traditional TDE scheme. Moreover, in fast fading channels, the traditional RAKE receiver has been proven to be less efficient than

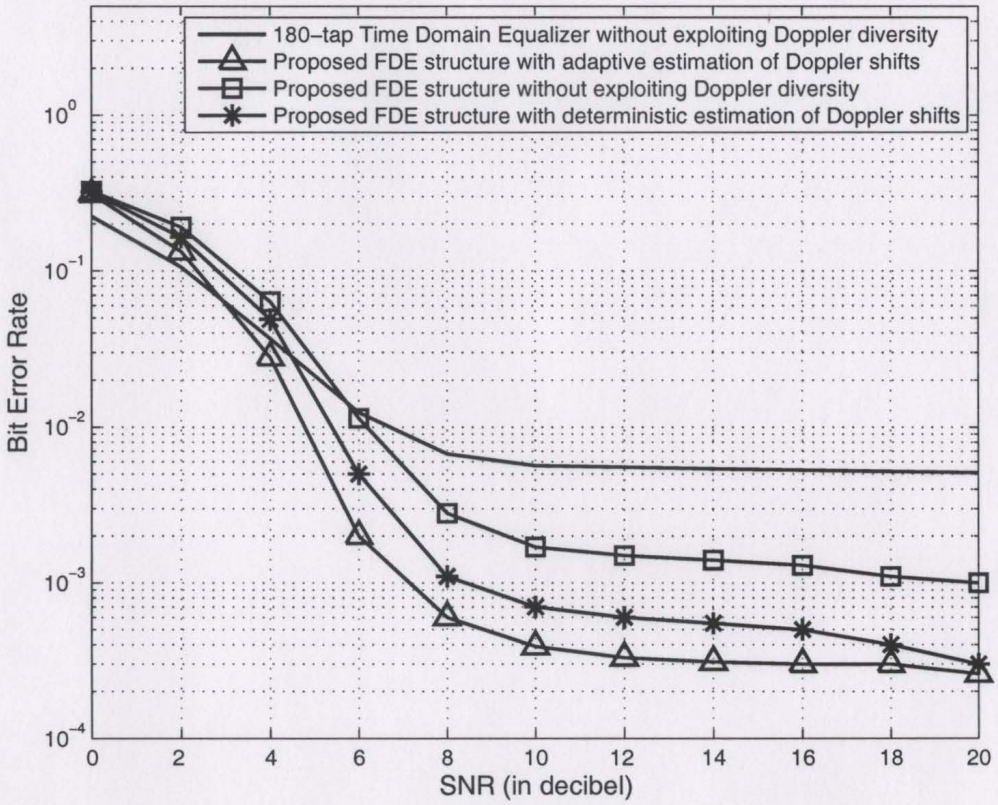

Figure 4.17: The BER performance of proposed FDE-based receiver structure in doubly selective channels where the velocity of the mobile station is 40km/hr

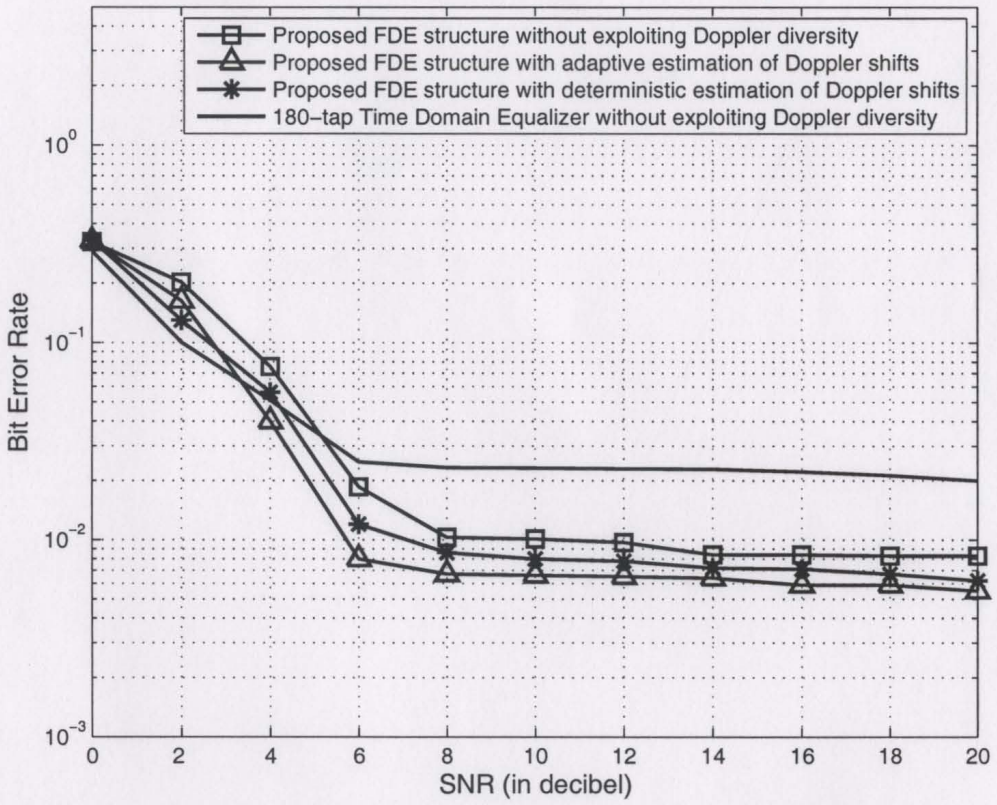

Figure 4.18: The BER performance of proposed FDE-based receiver structure in doubly selective channels where the velocity of the mobile station is 80 km/hr

both FDE-based and TDE-based receiver architecture [38]. Therefore, we do not include the performance curve of a traditional RAKE receiver.

4.2 Complexity Analysis

In this section, we study the complexity of an algorithm in terms of the number of multiplications required. Assume that the length of the transmitted frame is N. In DS-CDMA systems, the FDE requires three Fourier transform operations. Two of them are used for equalization and the other one is used for converting the CIR from time domain to frequency domain. This is in addition to the N complex multiplications required for equalization. Given that the complexity of a N-point DFT is $O(N\log_2 N)$, the total complexity of the FDE is $3P\log_2 N + N$ for DS-CDMA systems, where P denotes the length of each subframe. Moreover, the Doppler diversity can be easily exploited by linearly increasing the complexity of the FDE by adding more FDE branches. Hence, the complexity of the FDE-based equalization scheme is in the order of $O(N\log_2 N)$. In OFDM systems, the FDE requires two Fourier transform operations. This is in addition to the N complex multiplications required for equalization. Therefore, the total complexity of the FDE is $2N\log_2 N + N$ for OFDM systems. The complexity of the FDE in OFDM systems is also in the order of $O(N\log_2 N)$. In contrast, a time domain equalizer requires a direct inversion of a $N \times N$ matrix, whose complexity is to the order of $O(N^3)$ [47]. In addition, the complexity of a traditional RAKE receiver is to the order of $O(N^2)$ [39]. The proposed FDE-based receiver outperforms the TDE and RAKE-based receiver in both complexity and performance.

Due to the computational similarity and iterative nature of the proposed generic receiver architecture, this architecture is extremely suitable for the iterative approach

of implementation [48]. The algorithmic dimension of reconfigurability of the proposed algorithms can be well combined with the inherent hardware dimension of reconfigurability of the iterative approach to provide a great implementation flexibility. Therefore, the proposed receiver architecture is well switched to composite radio receivers.

4.3 Summary

In this section, we evaluate the performance of the proposed adaptive channel estimation algorithms by simulations. The simulation results show that the proposed algorithms can provide high accuracy. Based on the proposed channel estimation algorithms, the FDE-based receiver can provide good performance with low cost compared with traditional TDE-based receivers and Rake receivers.

Chapter 5

Conclusions and Future Work

5.1 Conclusions

Software defined radio (SDR) technology is an ideal solution to meet the requirements of the convergence of multiple wireless networks. DS-CDMA and OFDM systems are viewed as the most promising canditates for the next generation wireless technologies. The traditional Rake receiver used in DS-CDMA systems and FDE-based receiver used in OFDM systems have significantly different structures, especially in the channel equalization module, which makes it difficult to implement in a traditional DS-CDMA/OFDM receiver via SDR technology. The frequency domain equalization in OFDM systems is a low-cost equalization scheme with high-performance, while the Rake receiver in DS-CDMA systems is computationally burdensome and suffers from significant performance degradation in fast fading channels. Therefore, in this thesis, we develop a highly efficient FDE-based receiver architecture for DS-CDMA systems, based on which a generic FDE-based radio receiver in DS-CDMA/OFDM composite radio environment can be achieved.

Fighting against fast fading effect has become one of the most challenging tasks

of next generation wireless networks. In this thesis, we propose a FDE-based receiver architecture exploiting Doppler diversity in DS-CDMA systems. Firstly, by utilizing the basis expansion model, an adaptive method to better estimate the Doppler shift of each Doppler subpath is developed. This algorithm, which is based on the Expectation-Maximization (EM) method, can estimate Doppler shifts for real-time applications. Simulation results have shown that this algorithm outperforms the traditional deterministic method of estimating Doppler shifts. Secondly, to further improve the accuracy of channel equalization, we propose a frequency domain joint estimation algorithm of synchronization parameter and channel impulse response, which can be closely incorporated into a FDE-based receiver. When it is used together with a FDE, this joint estimation algorithm can provide fast convergence and better performance than the traditional equalization schemes.

By including the proposed adaptive estimation algorithms of Doppler shifts, synchronization parameters, and CIR, a FDE-based receiver is developed to exploit Doppler diversity in frequency domain. Simulation results have demonstrated that this receiver architecture features a good performance when compared with the performance of other traditional receiver architectures.

Based on the proposed FDE-based receiver architecture for DS-CDMA systems, a generic one-tap multiplier-based FDE scheme is eventually proposed to achieve a receiver architecture with better adaptivity and flexibility via the SDR technology. Simulation results have proven that the proposed generic FDE scheme can provide high performance and low computational complexity in both DS-CDMA and OFDM systems. With a generic channel equalization scheme, the proposed receiver architecture is an ideal candidate of the generic radio receiver for the next generation network.

5.2 Future Work

In our research, we proposed EM-based channel estimation algorithms for Doppler shifts, synchronization parameter and channel impulse response in DS-CDMA systems. To improve our research, the following issues will be further investigated:

1. More theoretical analysis will be included in the performance analysis section. Although we have provided plenty of simulation results, a complete theoretical analysis is still absent. To evaluate the MMSE performance, the corresponding Cramer-Rao Lower boundaries (CRLB) will be derived.

2. The proposed algorithms will be improved. EM-based algorithms will encounter the threshold problem as SNR increases. Therefore, the MMSE performance of proposed algorithms can not reach the CRLB at high SNR. To mitigate this problem, alternative algorithms are desired in relatively high SNR environment.

3. The implementation issues will be addressed. So far, our research only includes the development of a generic receiver architecture. To prove the efficiency of the proposed receiver architecture, a software implementation following the SCA3.0 protocol is desired.

The above issues either are currently under investigation or will be addressed in the future research.

References

[1] P. Burns, *Software Defined Radio for 3G*, 1st ed. Boston London: Artech House, 2003.

[2] J. Standards, *Software Communications Architecture.*

[3] L. Harju and J. Nurmi, "A programmable baseband receiver platform for wcdma/ofdm mobile terminal," vol. 1, New Orleans, La, USA, Mar. 2005, pp. 141–145.

[4] ——, "A baseband receiver architecture for umts-wlan interworking applications," vol. 2, Alexandria, EGYPT, 2004, pp. 678– 685.

[5] O. Simeone, Y. Bar-Ness, and U. Spagnolini, "Pilot-based channel estimation for ofdm systems by tracking the delay-subspace," *IEEE Transactions on Wireless Communications*, vol. 3, no. 1, pp. 315–325, jan 2004.

[6] H.-H. Chen and M. Guizani, *Next Generation Wireless Systems and Networks*, 1st ed. England: John Wiley, 2006.

[7] J. H.Reed, *Software Radio: A modern approach to radio engineering*, 1st ed. New Jersey: Prentice Hall, 2002.

[8] T. Ojanpera and R. Prasad, *Wideband CDMA for Third Generation Mobile Communications*, 1st ed. Boston, London: Artech House Pulblishers, 1998.

[9] O. M. Group, Tech. Rep.

[10] E. D., F. L., and Z. Z., "Recent developments in enabling technologies for software defined radio," *Communications Magazine, IEEE*, vol. 37, pp. 112–117, Aug. 1999.

[11] G. Ahlquist, M. Rice, and B. Nelson, "Error control coding in software radios: An fpga approach," 1999. [Online]. Available: citeseer.ist.psu.edu/ahlquist99error.html

[12] W. Y. Zou and Y. Wu, "Cofdm: An overview," *IEEE Transactions on Broadcasting*, vol. 41, pp. 1–8, Mar. 1995.

[13] W. T. Ng and V. K. Dubey, "On coded pilot based channel estimation for ofdm in very fast multipath fading channel," in *Proceedings of the 2003 Joint Conference of the Fourth International Conference on Information, Communications and Signal Processing, 2003 and the Fourth Pacific Rim Conference on Multimedia*, Singapore, Dec. 2003, pp. 859–863.

[14] G. K. Hikmet Sari and I. Jeanclaude, "Transmission techniques for digital terrestrial tv broadcasting," *Communications Magazine, IEEE*, vol. 33, pp. 100–109, Feb. 1995.

[15] H. Meyr, M. Moeneclaey, and S. A. Fechtel, *Digital Communication Recevers : Synchronization, Channel Estimation, and Signal Processing.* A Wiley-Interscience Publication, 1998.

[16] A. M. Sayeed and B. Aazhang, "Joint multipath-doppler diversity in mobile wireless communications," *IEEE Transactions on Communications*, vol. 47, no. 1, Jan. 1999.

[17] T. S. Rappaport, *Wireless Communications : Principles and Practice*, 2nd ed. MA: Addison-Wesley, 1972.

[18] J. G. Proakis, *Digital Communications*, 4th ed. MA: Addison-Wesley, 1972.

[19] S. Glisic, *Advanced Wireless Communications : 4G Technologies*, 1st ed. England: John Wiley, 2004.

[20] T. Pollet and M. Peeters, "Synchronizatin with dmt modulation," vol. 20, pp. 569–571, Nov. 1999.

[21] K. Witrisal, *OFDM Air-Interface Design for Multimedia Communications*, ph.d. thesis ed. Delft University of Technology, Apr. 2002.

[22] I. Koffman and V. Roman, "Broadband wireless access solutions based on ofdm access in ieee 802.16," vol. 20, pp. 569–571, Nov. 1999.

[23] S. Coleri, M. Ergen, A. Puri, and A. Bahai, "Channel estimation techniques based on pilot arrangement in ofdm systems," *IEEE Transactions on Broadcasting*, vol. 48, pp. 223–229, Sept. 2002.

[24] B.Yang, Z. Cao, and K.B.Letaief, "Analysis of low-complexity windowed dft-based mmse channel estimator for ofdm systems," *IEEE Transactions on Communications*, vol. 49, pp. 1977–1987, Nov. 2001.

[25] M. B. Pursley, "Performance evaluation for phase-coded spread-spectrum multiple-access communications : System analysis," *IEEE Transactions on Communications*, vol. COM-25, pp. 795–799, Aug. 1977.

[26] D. E. Borth and M. B. Pursley, "Analysis of direct-sequence spread spectrum multiple-access communication over rician fading channels," *IEEE Transactions on Communications*, vol. COM-27, pp. 1566–1577, Oct. 1979.

[27] C. S. Gardner and J. A. Orr, "Fading effects on the performance of a spread spectrum multiple-access communication system," *IEEE Transactions on Communications*, vol. COM-27, pp. 143–149, Jan. 1979.

[28] J. G. Proakis and M. Salehi, *Communication Systems Engineering*, 2nd ed. Prentice Hall, 2002.

[29] J. W. C. and JUN., *Microwave mobile communications*, 1st ed. New York: Wiley, 1974.

[30] P. Dent, G. E. Bottomley, and T. Croft, "Jakes fading model revisited," *Electronics Letters*, vol. 29, pp. 1162–1163, June 1993.

[31] O. Rousseaux, G. Leus, and M. Moonen, "Estimation and equalization of doubly selective channels using known symbol padding," *IEEE Transactions on signal processing*, vol. 54, no. 3, Mar. 2006.

[32] M. Jeruchim, P. Balaban, and K. S. Shanmugan, *Simulation of Communication Systems*, 1st ed. New York: Plenum Press, 1992.

[33] G. B. Giannakis and C. Tepedelenlioglu, "Basis expansion models and diversity techniques for blind identification and equalization of time-varying channels," *Proceedings of the IEEE*, vol. 86, no. 10, Oct. 1998.

[34] G. D'Aria, F. Muratore, and V. Palestini, "Simulation and performance of the pan-european land mobile radio system," *IEEE TRANSACTIONS ON VEHICULAR TECHNOLOGY*, vol. 41, pp. 177–189, May 1992.

[35] G. D'Aria, R. Piermarini, and V. Zingarelli, "Fast adaptive equalizers for narrow-band tdma mobile radio," *IEEE TRANSACTIONS ON VEHICULAR TECHNOLOGY*, vol. 40, pp. 392–404, May 1991.

[36] D. K. Kim and P. Park, "Adaptive self-orthogonalizing per-tone decision feedback equalizer for single carrier modulations," *IEEE Signal Processing Letters*, vol. 13, pp. 21–24, Jan. 2006.

[37] N. Benvenuto and S. Tomasin, "On the comparison between ofdm and single carrier modulation with a dfe using a frequency-domain feed forward filter," *IEEE Transactions on Communications*, vol. 50, no. 6, pp. 947–955, 2002.

[38] I. Martoyo, T. Weiss, F. Capar, and F. K. Jondral, "Low complexity cdma downlink receiver based on frequency domain equalization," vol. 2, Orlando, Florida USA, Oct. 2003, pp. 987–991.

[39] K. L. Baum, T. A. Thomas, F. W. Vook, and V. Nangia, "Cyclic-prefix cdma: An improved transmission method for broadband ds-cdma cellular systems," vol. 1, Orlando, USA, Mar. 2002, pp. 183– 188.

[40] A. S. Madhukumar, F. Chin, Y.-C. Liang, and K. Yang, "Single carrier cyclic prefix-assisted cdma system with frequency domain equalization for high data rate transmission," *EURASIP Journal on Wireless Communications and Networking*, vol. 2004, no. 1, pp. 149–160, 2004.

[41] K.-C. Ga, "Path searcher for a wcdma rake receiver," in *Freescale Semiconductor Inc. Application Note*, http://www.freescale.com/files/dsp/doc/appnote/AN2252.pdf, Mar. 2005.

[42] P.-Y. Tsai and T.-D. Chiueh, "Frequency-domain interpolation-based channel estimation in pilot-aided ofdm systems," *IEEE Transactions on Communications*, vol. 49, pp. 420–424, Nov. 2004.

[43] J. Cai, X. Shen, and J. W. Mark, "Em channel estimation algorithm for ofdm wireless communication systems," *The 14th IEEE 2003 International Symposium on Personal, Indoor and Mobile Radio Communication Proceedings*, pp. 804–808, 2003.

[44] J. H. Lee, J. C. Han, and S. C. Kim, "Joint carrier frequency synchronization and channel estimation for ofdm systems via the em algorithm," *IEEE Transactions on Vehicular Technology*, vol. 55, pp. 167–172, Jan. 2006.

[45] J.-J. van de Beek, M. Sandell, and P. O. Borjesson, "Ml estimation of time and frequency offset in ofdm systems," *IEEE Transactions on Signal Processing*, vol. 45, pp. 1800–1805, 1997.

[46] Y. V. Zakharov, V. M. Baronkin, and T. C. Tozer, "Ml frequency estimation in systems with transmit diversity: Pilot signals, complexity, and accuracy," in *IEEE Personal, Indoor and Mobile Radio Communications Conference (PIMRC)*, Barcelona, Spain, Sept. 2004.

[47] L. Mailaender, "Low-complexity implementation of cdma downlink equalization," *Proceeding of the Second International Conference on 3G Mobile Communication Technologies*, pp. 396–400, Mar. 2001.

[48] I. Krikidis, J.-L. Danger, and L. Naviner, "An iterative reconfigurability approach for wcdma high-data-rate communications," *Wireless Communications, IEEE*, vol. 13, pp. 8–14, 2006.